ELECTRICAL PROPERTIES OF QUENCH-CONDENSED THIN FILM

A Thesis

by

KYOUNGJIN LEE

Submitted to the Office of Graduate Studies of
Texas A&M University
in partial fulfillment of the requirements for the degree of

MASTER OF SCIENCE

August 2007

Major Subject: Physics

ELECTRICAL PROPERTIES OF QUENCH-CONDENSED THIN FILM

A Thesis

by

KYOUNGJIN LEE

Submitted to the Office of Graduate Studies of
Texas A&M University
in partial fulfillment of the requirements for the degree of

MASTER OF SCIENCE

Approved by:

Chair of Committee,	Winfried Teizer
Committee Members,	Joseph Ross
	Hong Liang
Head of Department,	Edward S. Fry

August 2007

Major Subject: Physics

ABSTRACT

Electrical Properties of Quench-Condensed Thin Film. (August 2007)

Kyoungjin Lee, B.S., Korea Military Academy

Chair of Advisory Committee: Dr. Winfried Teizer

Electrical properties of thin film have been an issue of interest for a long time and there are many applications in contemporary industry. Interesting characteristics, such as a metal-insulator transition and superconductivity, were investigated and applied to manufacturing of various electrical devices. In this line of study, many experimental techniques have been introduced for precise measurement of the properties of thin film. Quench-condensation is one of the important techniques in the research of thin films.

To facilitate this research, we built a quench-condensation apparatus which can be used for a variety of experiments. The apparatus was designed for the fabrication of ultra-thin film and the in-situ measurement at low temperature. The apparatus was shown to operate well for the fabrication of thin films while monitoring the growth in-situ. As a part of the preliminary research, we measured the electrical properties of aluminum thin films at liquid nitrogen temperature by using this apparatus. An investigation of the thickness dependent conduction properties was successively performed in-situ. Experimental data showed agreement with theory, in particular the electrical conduction model of Neugebaur and Webb.

DEDICATION

To my God and Family and Friends

ACKNOWLEDGMENTS

This thesis would not have been possible without the help and support of numerous people. I would like to express my sincere gratitude to the chair of my committee, Dr. Winfried Teizer, for helping me with the details and in many other ways. I am very grateful to my committee members, Dr. Joseph Ross and Dr. Hong Liang who provided useful suggestions, conversations, and encouragement. I am also grateful to Dr. Glenn Agnolet for his advice, help and encouragement. I also would like to thank Kyongwan Kin for his devoted help, advice and encouragement. I would like to thank Dr. Zuxin Ye and Dr. Daya Rathnayaka who helped me with good advice on the experiment. I also wish to thank Layne Wylie for his devoted efforts and help on the experiment. I am also grateful to all faculty members in the Physics Department in Texas A&M.

I sincerely thank my colleagues in NanoLab. I would like to thank my fellow graduate students in the Physics Department. I also would like to extend my thanks to my fellow graduate students at Texas A&M University.

I wish to express my deepest gratitude to my god and family who have shown an enduring and wholehearted support.

TABLE OF CONTENTS

Page

Page

LIST OF FIGURES

Page

LIST OF TABLES

Page

CHAPTER I

INTRODUCTION

1.1 Motivation

Materials have some interesting characteristics when they are in 2D thin film form, for example, they can show a thickness or magnetic field driven metal-insulator transitions [1, 2] or superconductivity in the 2D regime [3, 4]. It is essential to use some special techniques for such an experiment. For that reason, we designed and constructed an experimental apparatus that can make high quality samples, using quench condensation.

1.2 Research Objective

The objective of this project is to measure the electrical conductivity of 2 dimensional (2D) aluminum and nickel thin films deposited at low temperature using a home-built quench-condensation apparatus. 2D thin films have been of great interest for several decades and many theoretical models have been proposed [5~11]. In most experiments metallic films are evaporated at room temperature and then cooled on a substrate [12~14]. We made an apparatus that can be immersed into liquid helium and then perform evaporations at low temperature. We have performed an in-situ experiment with this newly designed apparatus on the 2D conductivity of thin films.

This thesis follows the style of Physical Review Letters.

CHAPTER II

BACKGROUND

Materials have many interesting properties when they are in form of a very thin film. They have distinguishable physical characteristics and significantly different electrical properties depending on the growth process [14~16]. Many physical models have been proposed to describe the relation between physical characteristics and electrical properties [5~11]. Typically, they can be categorized into classical and quantum mechanical models. For thin films with large grains the electrical conduction can be explained by thermal activation and tunneling effects [14]. On the other hand, for ultra thin films with small granular grains, experimental results show anomalous behavior that is not expected from classical models [3]. In this chapter, we will focus on understanding the electrical properties and the growth process of thin films. Furthermore, we will introduce the basic techniques of thin film fabrication for understanding the importance of our experimental technique, which is applied to get the expected experiment results on the electrical properties of thin films.

2.1 Thermal Evaporation

Thermal evaporation is the simplest deposition technique to deposit various materials by a physical deposition process. Materials are heated to evaporate by applying a high electric current and then deposited onto a substrate to form a thin film. The evaporation occurs in a high vacuum where the mean free path of the incident atoms is much longer than the distance from the evaporation source to the substrate. Therefore, evaporated atoms are incident by ballistic motion and then deposit onto the exposed surface of a substrate forming a thin film.

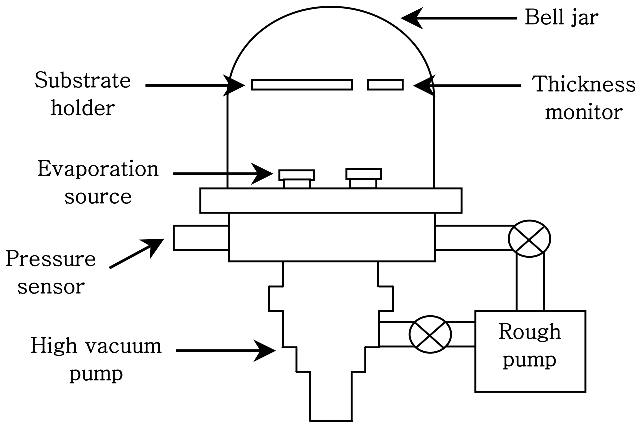

Figure 2.1 Schematic design of typical thermal evaporator

Figure 2.1 shows the schematic design of a typical thermal evaporator. The thermal evaporator consists of a vacuum chamber, pumping system, evaporation source, and monitoring equipment. For a typical thermal evaporator, at room temperature, a glass or stainless steel bell jar is commonly used as a vacuum chamber. The vacuum chamber is sealed to a stainless steel base plate with a rubber gasket. It is very important to maintain the condition of a high vacuum during the evaporation process since it critically affects the quality of the thin film by contamination, oxidization, reaction, and so on. Furthermore, atmospheric pressure also causes a change of the phase transition temperature. As the pressure is reduced, materials undergo a phase transition from solid to gaseous state at lower temperature. Such a phase transition allows more materials to evaporate, particularly if it has a high melting point. As an example, to evaporate nickel, we should increase its temperature up to 1525˚K at 10^{-4}torr. On the other hand, only 1200˚K is enough for an evaporation at 10^{-8}torr. Both rough pumps and high vacuum pumps form the basic pumping system to produce a high vacuum inside the chamber. A rough pump is capable of reaching a pressure of at most $P=10^{-4}$torr, while a high vacuum pump reaches $P=10^{-6}\sim10^{-8}$ torr. Generally, a diffusion pump, a turbo molecular pump or a cryopump is used for high vacuum pumping. Materials to be evaporated (evaporant) are held by evaporation sources, like a crucible, boat or wire coil. Tungsten wire is commonly used as an evaporation source for materials like aluminum, nickel, chromium, gold, lead, and so on. A quartz crystal microbalance (QCM) is used to measure the thickness of the sample and an ion gauge monitors the vacuum. Additional monitoring equipment can be added depending on experimental purposes.

2.2 Quench Condensation

The technique of quench-condensation has been developed to evaporate a thin film of some reactive materials in an ultra-high vacuum which are subsequently cooled down to a temperature of liquid helium (~4.2°K). In this technique, while monitoring the film’s thickness and resistance, various thicknesses of thin films are grown by sequential evaporation onto a cryogenic substrate without breaking the ultra-high vacuum conditions [17]. This method makes it possible, for example, to experimentally measure a metal-insulator transition in a thin film, which has two dimensional resistance and thickness dependence. In addition, this technique can be applied to producing a thin film with very high quality [17, 18]. Figure 2.2 shows the general design of a quench condensation system. This system has cold substrates that are maintained at 4.2K for rapid quenching of the evaporant. Generally the evaporation source is installed at T > 4.2K, while the path between the substrate and the source is blocked by a shutter.

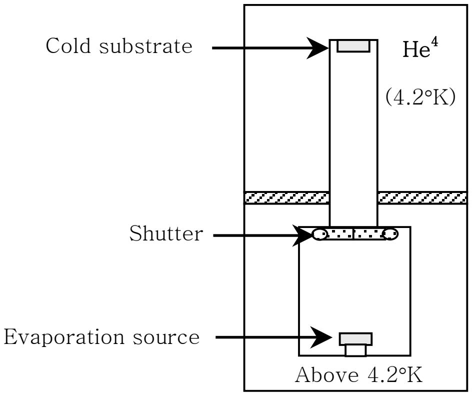

Figure 2.2 Schematic design of quench condensation system

2.3 Growth Process of a Thin Film

2.3.1 Introduction

In order to obtain thin films with prescribed physical characteristics, it is required to understand the physical mechanism of its deposition process. Thin film deposition is a multi-phenomenon process. While atoms are kinetically colliding with the substrate, one can observe phenomena such as physical adsorption and nucleation, growing, ripening, and so on. Atoms sometimes nucleate at the surface of a substrate and then form a cluster that makes a discontinuous film by forming what is called islands. Clusters are developed and increase in area until they form a continuous film. Figure 2.3 is a transmission electron micrographs of ultra-thin Au film, which shows progression from discontinuous to network stages [14].

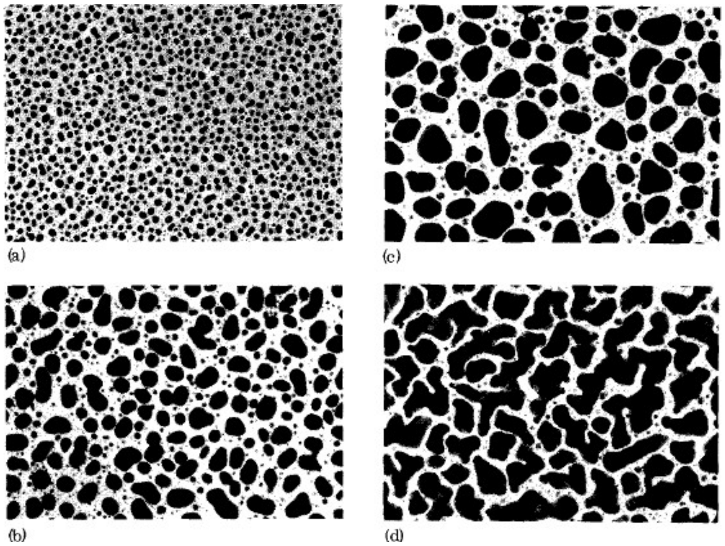

Figure 2.3 Electron micrographs of thin Au films.
Deposited at 0.5Å/sec. Thickness are (a) 10 Å, (b) 40Å, (c) 60 Å, (d) 150 Å
[From L. L. Kazmerski and D. M. Racine, J Appl Phys, vol. 46, 791 (1975)][14]

2.3.2 Adsorption

Atoms do not always stick to the surface of a substrate but they scatter or re-evaporate if a atom has comparatively large kinetic energy [15, 19]. Evaporated atoms interacts with other incident atoms while exchanging energy with the substrate until they are condensed on the surface. Ideally, the atom should suddenly lose enough energy after a collision to stay on the surface of the substrate. Figure 2.4 shows the relation between the kinetic energy of an evaporated atom and the potential energy on the surface of the substrate. The potential energy is a synthesized effect that includes the interaction energies of atom-atom and atom-substrate, as seen in Figure 2.4. When a atom loses its energy from A to B then it scatters. On the other hand, when a atom loses its energy from A to C or D then is can stay on the surface of the substrate. Quench condensation can take place when an atom loses its energy from *A* to *D*. Of course, the reversed process also happens from *C* to *B* by re-evaporation that will be mentioned in the next section. This is summarized in Table 2.1.

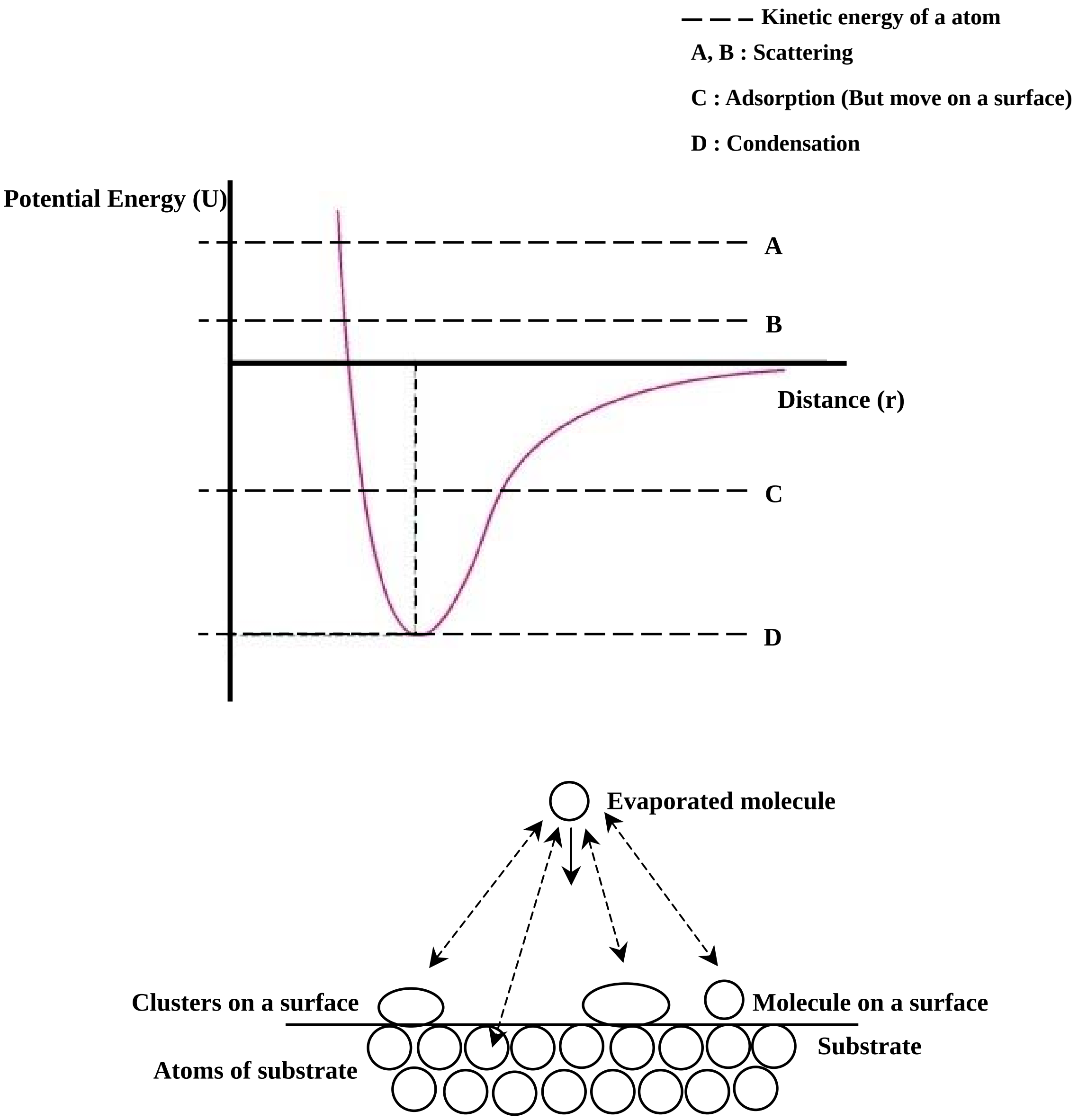

Figure 2.4 Potential energy versus distance from the surface of substrate (up) and interactions between atoms (down)

Table 2.1 Activity of an evaporated atom depend on its kinetic energy

Process	Action	Energy	Remarks
A → B	Scattering	K > U	Prominent for laser ablation
A → C	Adsorption	K < U	General evaporation
A → D		K << U	Quench-condensation
C → B	Re-evaporation	K > U	Escape form the surface

2.3.3 Nucleation

An incident atom can undergo a mass transport process after colliding with the surface of the substrate [15, 20]. Incident atoms form small grains by nucleation with other atoms. But some atoms do not participate in formation of grains but instead transport their mass by dissolution into the substrate, capturing at a defect site, re-evaporation. Nucleation is an isothermal phase transition from the vapor state to condensed state. Grains are statistically distributed over the substrate surface and grow in size to form clusters.

2.3.4 Growing

Clusters migrate themselves over the surface and interact with other clusters. Clusters grow and merge with other clusters by either liquid or solid like adhesion. This can be explained with their surface energy [14, 15]. Small particles have large surface energy because they have large surface area to volume ratio. Intrinsically, a system follows a physical process to reduce the total surface energy. The total surface energy of the system decreases when small clusters coalesce into larger clusters. After merging, the surface energy is decreased due to the new surface area being less than the summed surface area of two. Figure 2.5 shows a schematic of this process. During this process, clusters grow and coalesce to form islands on thin film surface and then these Islands continue to coalesce until form a continuous film.

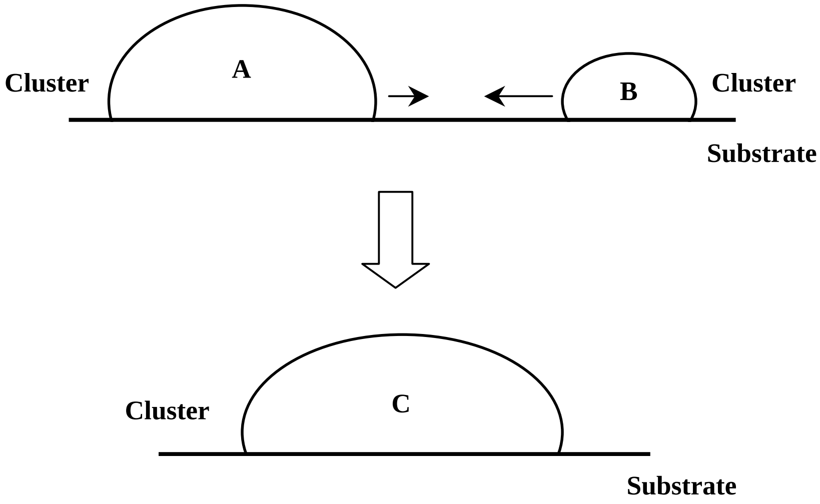

Figure 2.5 Schematic of coalescence process ($S_A + S_B > S_C$)

2.3.5 Ripening

A film initially grows in clusters but it starts ripening when it stops to form new islands. This happens when the evaporation rate is sufficiently low or evaporation is stopped. Ripening is the process that small clusters start to disappear to minimize the surface energy of a thin film by a similar mechanism to coalescence of clusters [15, 21]. The thin film reduces the surface energy by interaction of islands. During the ripening clusters undergo surface diffusion and coalescence to reduce the surface energy of thin film. Small clusters shrink and their number is reduced during the ripening. On the other hand, the large clusters increase and grow by coalescing with small clusters. Figure 2.6 shows AFM images of PbSe which shows this process [21].

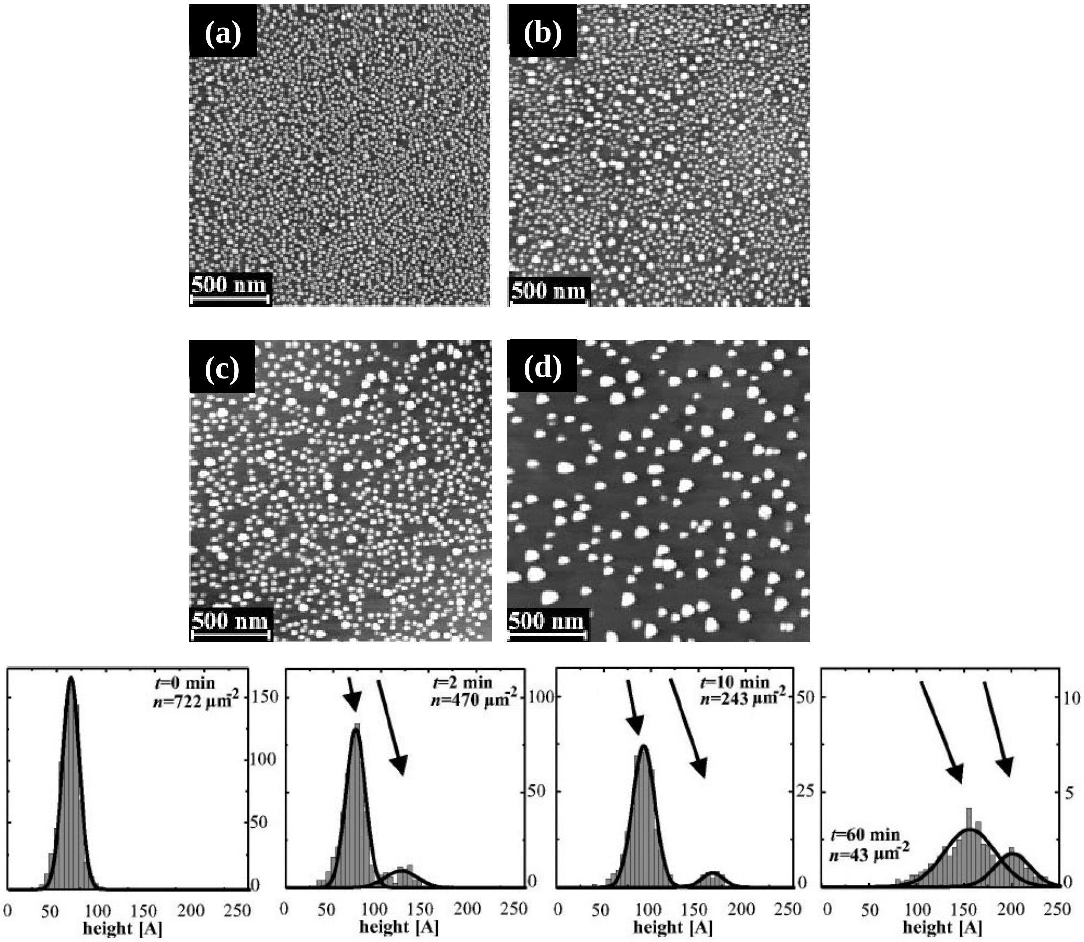

Figure 2.6 AFM Images of PbSe dots which shows ripening process
(Plots show density of dots and Gaussian distribution of height)
[From A. Raab and G. Springholz, App. Phys. Lett. 77, 2991 (2000)] [21]

2.3.6 Considerations on Thin Film Deposition

The films typically become continuous at average thickness that depends on many experimental conditions. As we have seen at the growing process of thin films, there are many factors that should be considered for thin film deposition. Typical considerations are:

the evaporation rate and the temperature of substrate, the type of material to be evaporated (evaporant) and substrate, and so on. The island size significantly depends on the evaporation rate and the temperature of substrate. Thin films have larger island size for higher evaporation rates or substrate temperatures since the surface mobility of clusters is enhanced with increasing surface energy [16]. The specific of evaporant also affects the deposition of a thin film. As a good example, gold has poor adhesion compared to other materials so it is difficult to form a thin film on silicon or a glass substrate. Therefore, we should pre-evaporate germanium, chromium or titanium to form a gold thin film on the substrate. Besides, the nature of substrate also affects the thin film deposition since it has varying topology and the adhesion depends on its character. Porousness and adhesion of the substrate affects the saturation and nucleation of atoms that affects the island size of thin film. Roughness and defects of the surface affects the uniformity of a thin film. Chemical stability and impurities of the substrate also affects the properties of a thin film [16].

2.4 Electrical Properties of Thin Films

2.4.1 Introduction

A material has many interesting properties when it is in form of a thin film. A metal can have nonmetallic properties in form of a very thin film [22]. On the other hand, an insulator can have metallic properties when it is in form of a thin film in some unique circumstances [23]. Besides, thin films of magnetic materials can show a metal-insulator transition when tuned by a magnetic field [1, 2]. A superconducting thin films like Pb, Al, Sn has nonmetallic property when it is very thin and then it transforms to a superconductor when grown to be thicker [22]. VO_2 shows a transition of its electronic properties from insulating to metallic [23]. Gd_xSi_{1-x} and Ni shows a magnetic field driven metal-insulator transition by application of a magnetic field [1~2]. Indeed, the electrical properties of a thin film are unique and sometimes quite different from materials in bulk condition. As we have seen at the thin film growth process, discontinuous growth of a thin film is a very important feature and we will use this as a starting point to explain the electric transport properties of a thin film.

2.4.2 Basic Models

In general, physical models for the electronic properties of a thin film can be categorized into two different ways by their physical condition. One is for a thin film forming islands, whose electronic properties are commonly explained by thermal activation and tunneling effects between the islands [5]. Another is for superconducting thin films, for which more quantum mechanical models are required to explain the electronic properties [3, 4].

Neugebauer and Webb proposed a simple model that explains conductivity of thin films with islands [5]. The model includes the electron transfer by the thermonic emission and the tunneling current between islands on a thin film. The model assumes that the thermonic emission dominates the transport mechanism when the separation of the islands is large. On the other hand, the tunneling current exceeds the thermonic current if the separation is small enough. For the thin film which is consisting of a planar array of many small, discrete metal islands of linear dimension *r*, separated by average distance *d* (inter island separation) the number of charged islands is described as

$$n = Ne^{-\varepsilon/kT} \tag{1}$$

where N is the total number of islands in the film and ε is the effective activation energy which is $\varepsilon \approx q^2/r$. q is the charge of a carrier (electron). The tunneling probability of an electron from one negatively charged island (i) to the neighboring islands (f) is

$$P \propto \int_{-\infty}^{\infty} D f_i (1 - f_j)\, d\varepsilon \tag{2}$$

where f is the Fermi function and D is the transmission coefficient. Figure 2.7 shows a conduction mechanism of thin film.

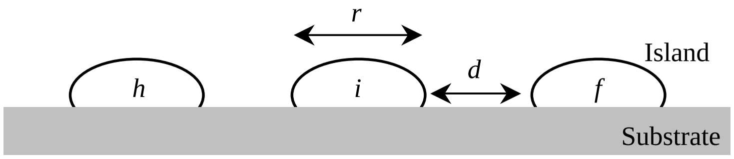

(a) Islands on a substrate

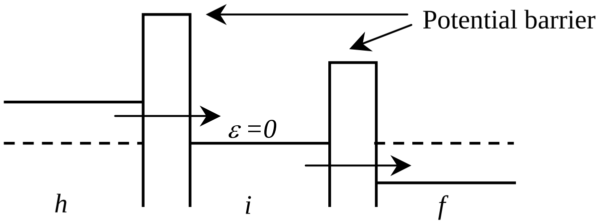

(b) Schematic of the conduction mechanism by Neugebauer and Webb [5]

Figure 2.7 Conduction mechanism of thin film

The conductivity is described as

$$\sigma \propto \frac{1}{r} d^2 q^2 D \exp\left(-\frac{q^2 / r}{kT} \right) \tag{3}$$

where D is the transmission coefficient, r is the effective island size and d is the distance between islands (inter island separation).

Figure 2.8 shows the experimental result of Kazmerski and Racine which investigated the conduction mechanism of ultra-thin (10~100Å) metalic films [14].

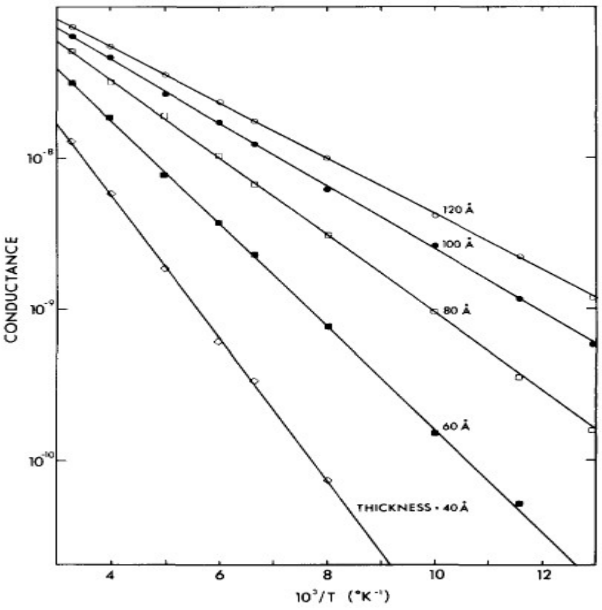

Figure 2.8 Experimental result of Kazmerski and Racine [14]
[From L. L. Kazmerski and D. M. Racine, J Appl Phys, vol. 46, 791 (1975)][14]

The experimental result shows agreement with the model of Neugebauer and Webb which predicts a linear dependence of the logarithmic scale of conductivity ($\ln\sigma$).

Another model, which was experimentally proven by A. Frydman and R.C. Dynes, explains the superconducting transition based on its critical behavior [3, 4]. For quench-condensed granular thin films, the sheet resistance versus temperature for $T<T_c$ follows and exponential behavior and can be expressed in the following way.

$$R = R_0 e^{T/T_0} \tag{4}$$

where R_o is the value of the resistance obtained by extrapolating the R-T curves to $T=0$ and T_0 is its temperature. Though the cause for this dependence is not fully understood, it turns out to be universal for two-dimensional (2D) granular superconducting thin films. In this model, the equation does not depend on the nature of the superconducting grains but only on the geometrical arrangement of the grains which is affected by the specifics of the thin film deposition.

2.4.3 Metal-Insulator Transition in a Thin Film

The electrical conductivity of a material can be changed from metal to insulator or vice versa by its physical condition. This transition is well known as metal-insulator transition and has been studied for a long time [24~31]. Scientists tried to understand its physical principles by studying some transitions from metal to insulator after Wilson gave a description of the difference between metals and insulators in 1931 [24]. The area of research has been broadened by development of experimental techniques and subsequently topics such as a magnetic field driven metal-insulator transition [1, 2], hole driven metal-insulator transition [23] were studied.

A Metal-insulator transition is a typical quantum phase transition which is generally described at T=0K while it is modified due to its temperature dependence at T≠0K [25]. We cannot clearly define the transition at T≠0K because it's boundaries are broadened by finite temperature. In this case, we cannot clearly define its metallic and insulating behaviors but materials can be described as a good or bad conductor (Figure 2.9).

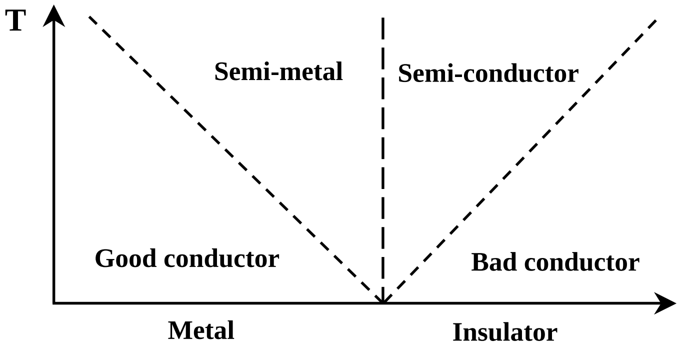

Figure 2.9 Metal-insulator transition as quantum phase transition
χ : External parameters like magnetic field and film thickness, and so on

For disordered 2D thin films, metallic and insulating behaviors can be defined through the temperature dependence of the electrical conductivity σ [1, 2]. If $\sigma_0 \equiv \sigma(T \to 0) > 0$ we designate this as metallic while we define insulating as $\sigma_0 \equiv \sigma(T \to 0) = 0$. The electrical conductivity σ is described as

$$\sigma(T) = \sigma_0 + \sigma_1 \times T^{1/2} + \sigma_2 \times T \tag{5}$$

where σ_0 is conductivity at T=0°K, $\sigma_1 \times T^{1/2}$ is the first–order correction due to Coulomb interaction and $\sigma_2 \times T$ is a corrections due to quantum back-scattering effect [1, 2].

CHAPTER III

QUENCH-CONDENSATION APPARATUS

As we discussed in the previous chapter, two-dimensional (2D) thin films were known to show very unique electrical properties that were successfully described based on quantum mechanical models. Until now, several methods have been used to deposit thin films at room temperature but these techniques were not enough to investigate the 2D electrical properties. In this case, samples were dominated by bulk properties including the thermal activation. On the other hand, the quench-condensation technique enabled the investigation of 2D thin film. We designed and built a very simple apparatus that can be immersed into liquid helium and then perform quench-condensation with in-situ measurement at low temperature.

3.1 Design Overview

Figure 3.1 shows the exterior view of an insertable cryostat and our apparatus. Our apparatus looks like a small cryostat for a storage dewar that is constructed for saving time and money. This types of apparatus allows quick turn around times, typically, a sample can be mounted and is ready to be measured in a few hours. In case of our apparatus, it has been designed not only for the measurement but also for the fabrication of a sample. Therefore it is adaptable to many applications and very convenient to use. Besides, the most important advantage of this particular design is that it enables the quench-condensation of thin film with in-situ measurement.

Figure 3.1 Exterior view of an insertable cryostat (left) and our quench-condensation apparatus (right)

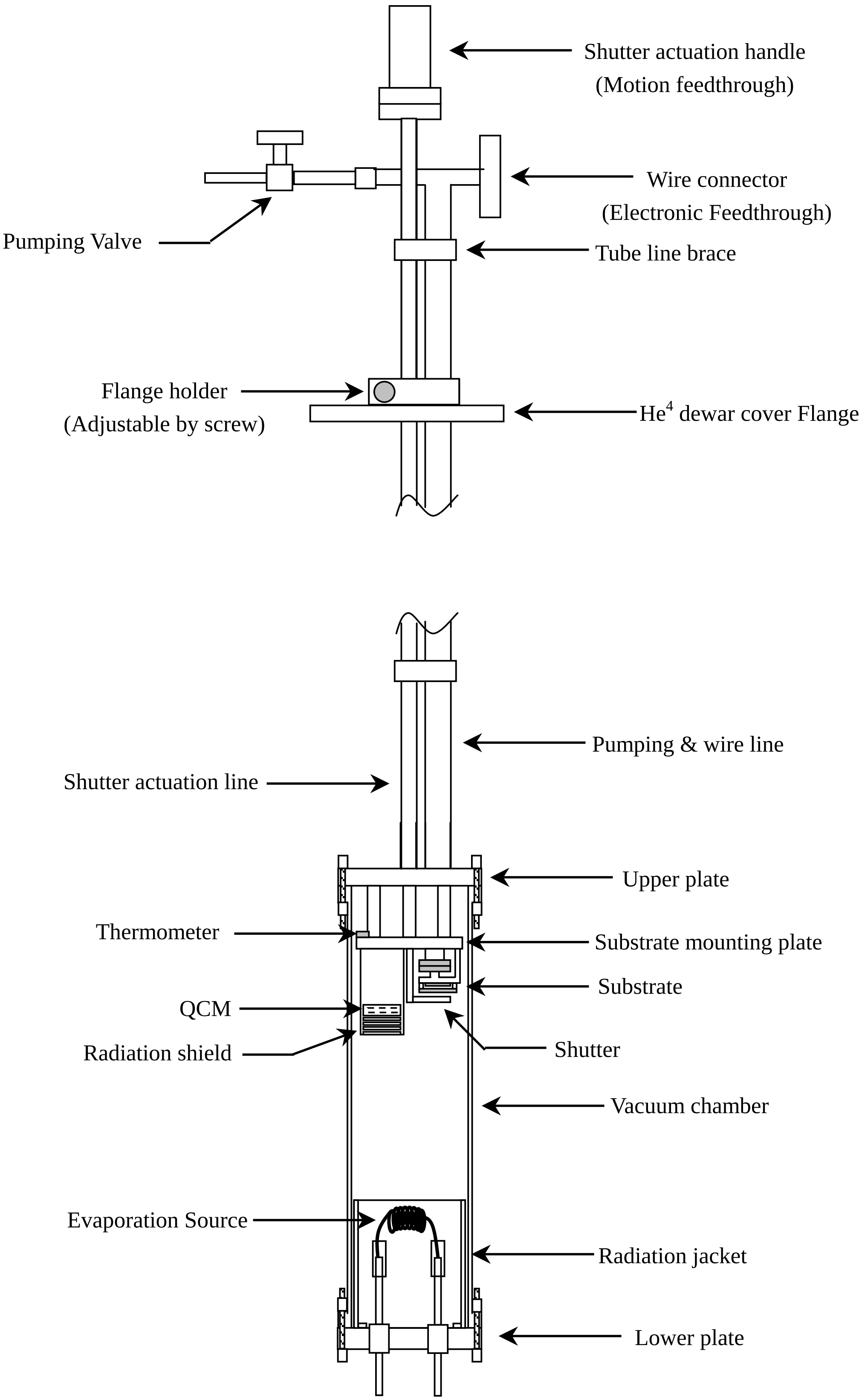

Figure 3.2 Schematics of our quench-condensation apparatus

Figure 3.2 shows the schematic design of our apparatus. This small quench condensation apparatus (SQCA) consists of a small chamber with a evaporation source components (the lower plate) and cold substrate components (the upper plate), two tubes with a flange holder, a pumping valve, a wire connector and a shutter actuation handle. The obvious constraint in this design is the dimension of the ^{4}He dewar that has a magnet at the bottom. The neck of our ^{4}He dewar is 3.4 inches in diameter. The distance from the top of the neck to the magnet is 117cm and the bottom of the dewar is 155cm as described at Figure 3.3. This distance from the top of the neck to the magnet determined the length of pumping lines and the diameter of the neck determined the size of flanges on the vacuum chamber.

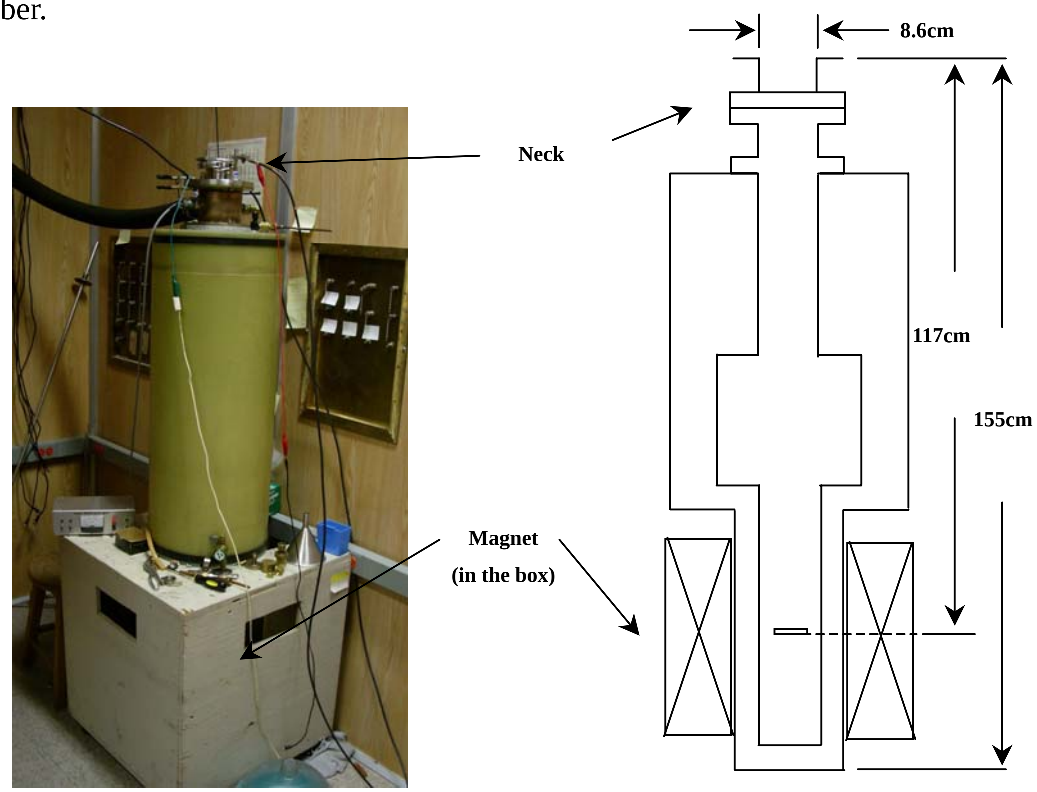

Figure 3.3 The exterior view and schematic dimensions of ^{4}He dewar

3.2 Construction Details

The evaporation chamber is made of stainless steel with diameter of 4.8cm and length of around 15.2 cm. The length of the evaporation chamber is determined to maintain a moderate evaporation rate while protecting the system from the heat radiation. Excessive length results in a poor evaporation rate and too short a length results in too much heat radiation on to the substrate that is undesirable for the thin film quality [32]. It is important to note that stainless steel was used for most parts of our apparatus, since the small thermal conductivity of stainless steel at low temperature ensures the successful operation although it is hard to machine in cryogenic instrument manufacture. For building a high vacuum instrument, it is useful that stainless steel has little outgasing and no diffusion of gas. At each end of the chamber, there are two flanges, which connect the upper and lower plate to mount the substrate and evaporation source, respectively. Flanges are designed for Indium O-rings and connected to the chamber by welding. Welding is one of the most reliable methods to combine two pieces of stainless steel. When connected by welding, the materials are homogeneous and less subject to stress from differential thermal contraction [33, 34]. Figure 3.4 shows a cross section of an Indium O-ring flange and view of flanges from above. An Indium O-ring uses simply thin indium wire wrapped in a circle with the ends twisted together. An Indium O-ring seal is easy to machine compared with that of copper or rubber seal, since it does not need an O-ring groove. One side of the flange can be easily sealed by an Indium O-ring.

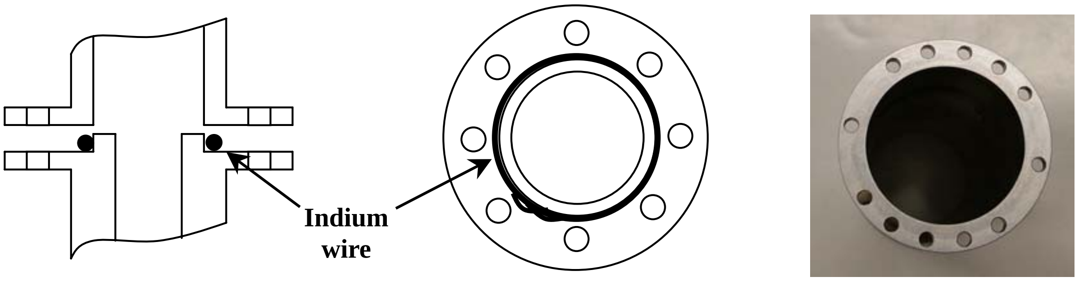

Figure 3.4 Indium O-ring flange

An Indium O-ring seal is reliable for a cryogenic seal unlike a rubber O-ring seal since rubber is no longer elastomeric[33] at low temperature. However one should be careful to use the Indium sealed apparatus for evaporation at room temperature as Indium melts at high temperature around 430K. This apparatus should be used only for certain materials that have low melting point when it is applied to room temperature evaporation. For example, aluminum can be evaporated at room temperature with the Indium O-ring sealed apparatus, while nickel cannot. Certainly, this is not a problem when using quench-condensation because the flange always remains at low temperature in that case. 8 holes for assembly and 4 holes for wire paths are drilled into the flange. 2 more holes are drilled into the flanges of the upper and lower plate in order to readily allow detachment after usage.

The upper plate with flange is connected to two tubes by welding as can be seen in Figure 3.2. We used thin-walled stainless steel tube because of its low thermal conductivity and high strength. One of the tubes is for the path of the shutter actuation rod and another is for the pumping line. Wires for measurement also pass through the pumping line. Figure 3.5 shows components of the upper plate. A substrate was placed on a 3.31cm-diameter circular shape substrate mounting plate that is directly connected to the upper plate with small spacer rod. We used OFHC copper for these parts because it is an excellent conductor and good for vacuum instrumentation. The substrate maintains a temperature of 4K because of this direct thermal connection to the chamber wall. A Cernox CX-1050 thin film resistance sensor is mounted on the backside of the substrate mounting plate. A Quartz Crystal Microbalance sensor (QCM) of 5MHz is attached at a small OFHC copper plate that is mounted on the substrate mounting plate. For protection, the QCM is radiation shielded with 4 copper baffles and a stainless steel box. A shadow mask is attached to the substrate by 0-80 screws and spacers. A shutter is made of stainless steel and attached to the shutter actuation rod by welding. The rod is made of stainless steel tube that is sealed into an other tube. 16 wires are connected to the substrate by two detachable 16-pin sockets.

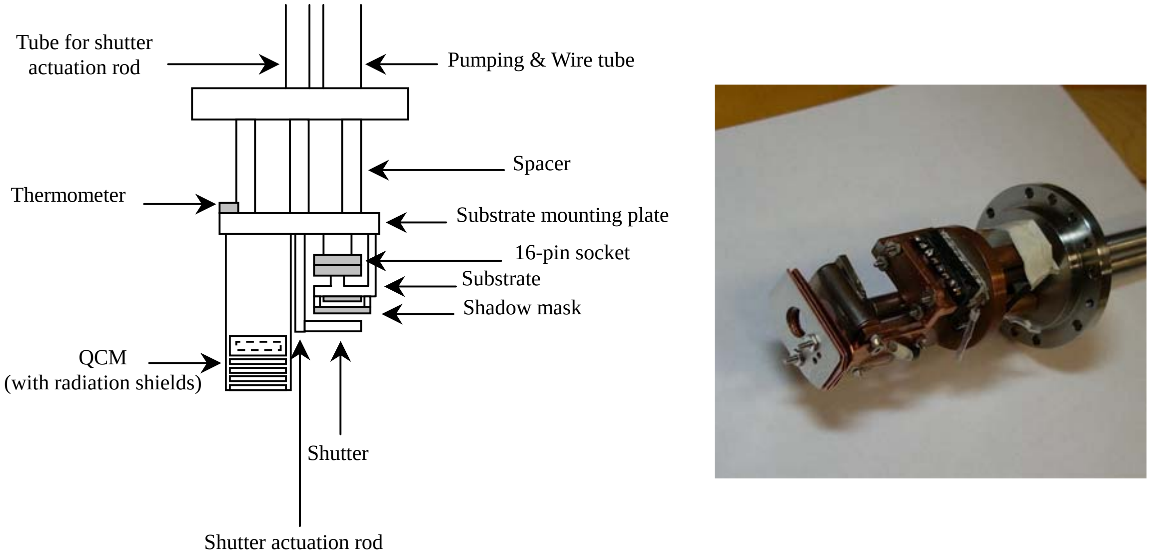

Figure 3.5 Upper plate components

Figure 3.6 shows the lower plate components. 4 electrical feedthroughs are welded to the lower plate for evaporation source holder. We used ISI 30 Amps high vacuum electrical feedthrough that consists of a copper electrode and alumina ceramic insulated stainless steel body. We connected evaporation filament to the electrodes by using commercial inline power connectors. It was possible to evaporate several different materials at the same time or sequentially by using 4 electrodes. An OFHC copper thermal radiation jacket is mounted to the lower plate to suppress thermal radiation from the evaporation source to the wall of the chamber.

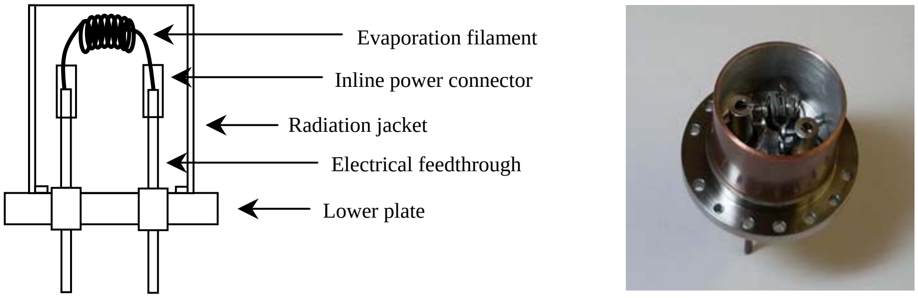

Figure 3.6 Lower plate components

A selection of correct wire is very important for cryogenic apparatus. We should reduce the heat flow into the apparatus while keeping good electronic conductivity. We used fine Manganin wires that have low thermal conductivity with appropriate resistivity of around 43~48 μΩ/cm at 4.2 ~295K. Wires are connected from the ISI Copper Flange multi-pin electronic feedthrough at the top of the tube to the electronic components at the lower plate (See Figure 3.7). 16 Manganin wires are used for measurement and heating, 4 wires are used for a thermometer. Suppressing noise is especially important for a sensitive measurement with high frequency. We used coaxial wires for the QCM to suppress noise during its sensitive measurement. Other wires are twisted in pairs to reduce noise.

Figure 3.7 shows the components on top of the SQCA. A MDC rotary motion feedthrough provides the control of shutter. Typical vacuum valve is used for pumping connection. Two copper gasket flanges are used for motion and electronic feedthrough that are attached on top of the tubes.

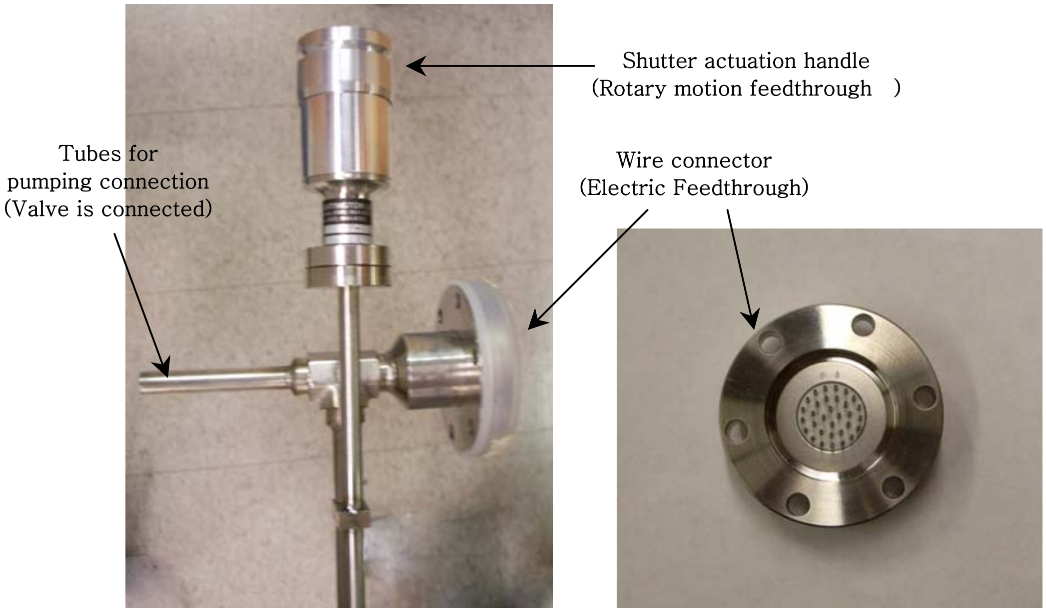

Figure 3.7 Components on top of SQCA

CHAPTER IV

EXPERIMENTAL ISSUES

The electrical properties of quench condensed thin films were compared with other samples that are evaporated at liquid nitrogen and room temperature. Quench condensation is achieved with the home-built quench condensation apparatus by immersing it into ^{4}He. The same apparatus was also used to perform the evaporation at nitrogen. On the other hand, the room temperature evaporations were done with a commercial thermal evaporator. All evaporations and measurements were performed in-situ except for those at room temperature. By using a superconducting magnet mounted in the ^{4}He dewar, the magnetic properties of samples can be measured. Figure 4.1 shows the schematic of experimental procedure.

4.1 Experimental Set-up and Procedure

4.1.1 Room Temperature Evaporation

Thin films were evaporated at room temperature with NRC 3114 commercial thermal evaporator. We deposited aluminum and nickel thin films in a form of bar with shadow mask. A commercial tungsten basket was used for the evaporation source. The evaporation rate was set to around 1Å/sec and vacuum pressure was maintained no more than 4.0×10^{-6} torr. We measured the conductivity of samples with the quench condensation apparatus at room and liquid nitrogen temperature, respectively.

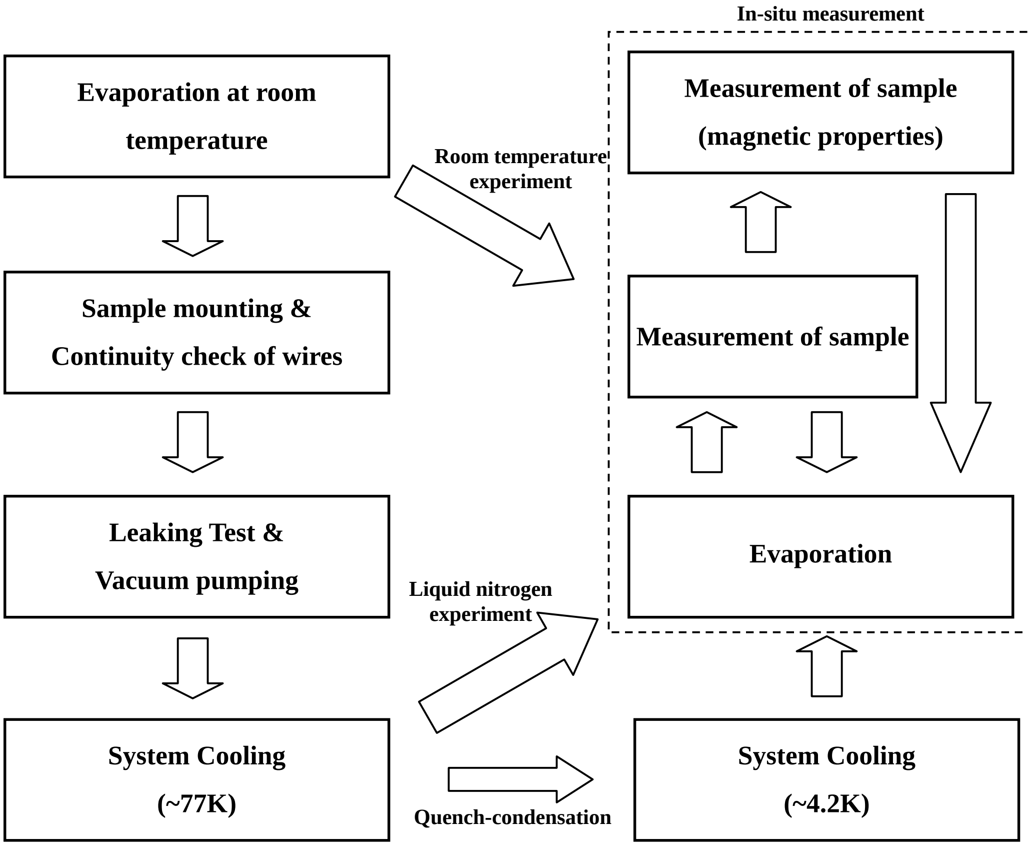

Figure 4.1 Schematic of experimental procedure

4.1.2 Evaporation at Liquid Nitrogen

The substrate was prepared for in-situ measurements. Before producing a high vacuum, the vacuum chamber was leak-tested with an Alcatel ASM 142 leak detector. The chamber was evacuated by using a defunct MS-9 Veeco leak detector which has a rough and a diffusion pump. To protect the vacuum system, two successive pumping steps were performed to reach no more than ~10^{-2} torr at first with the rough pump and then a typical limit of 10^{-6} torr with a diffusion pump respectively.

The electronic apparatus was connected to the quench-condensation apparatus before being immersed into a dewar. Two differential preamplifier (PAR™ MODEL 116, 117) and two multimeter (HEWLETT PACKARD 3457A, 3478A) were used for the 4-wire measurement of the sample and thermometer (Cernox CX-1050 thin film resistance sensor). A precision voltmeter (Guideline 9578) was used as an auxiliary apparatus for the measurement. A universal counter (HP 5315A) was used to measure the frequency of QCM for monitoring the thickness of the sample. A stabilized power supply (FARNELL INSTRUMENT L30-2) and a home made QCM oscillator were used to generate oscillations on the QCM. The frequency of the QCM and the initial resistance of thermometer were measured before immersing the apparatus into the dewar.

The vacuum pump was disconnected before immerse the apparatus into liquid nitrogen. The apparatus was cooled down to 77K over a period of ~20 minute to protect the electronic feedthrough at the bottom of vacuum chamber. An evaporation was performed by heating the evaporation source with a DC Power Supply (HP 6274B, maximum 60V and 15A). The sample was measured in-situ and then the sequential process of evaporation and measurement was repeated.

4.1.3 Quench-Condensation (at ^{4}He)

For a quench-condensation, there are additional processes required for evaporation. All of the processes were the same compared to liquid nitrogen temperature evaporation until immersing the apparatus into the dewar. However, the main difference is that, inside the dewar, the liquid nitrogen has been replaced by ^{4}He. After the dewar was cooed down to

77K, liquid nitrogen was removed by producing a pressure in the dewar with nitrogen gas and then ^{4}He was transferred. During this process, the ^{4}He level was monitored by measuring the resistance of superconducting wire installed inside of the dewar. A sample was evaporated when the apparatus reached the temperature of 4.2K. The measurement of its electrical properties was performed. In addition, the magnetic properties of the sample were measured by using a superconducting magnet which is installed at the bottom of the dewar.

4.2 Evaporation Source

It is very important choosing a suitable evaporation source to produce a high quality sample. To provide good conditions for evaporation, the source must support a material to evaporate at high temperature without allowing a chemical reaction or significant alloying between them. The appropriate value of electric current plays a critical role for the success of an evaporation. It determines the evaporation rate which affects the quality of the sample. Furthermore, the evaporation is influenced by both the shape and amount of material.

There are different types of evaporation sources for various purposes in thermal evaporation. Typical evaporation sources are made of the tungsten (W), tantalum (Ta), molybdenum (Mo) or carbon (C). Tungsten is the most typical source for thermal evaporation since it has the highest melting point (3695K) and the lowest vapor pressure [15]. This source, which has a low thermal expansion rate at high temperature, does not easily oxidize or alloy with other materials. Its resistivity is not larger than that of other evaporation sources, but increases with temperature. At room temperature, its resistivity is about 5.65 μΩ/cm where as it is 24.93 μΩ/cm at 1000K.

As mentioned before, the geometrical form of an evaporation source affects the evaporation process. The typical form is a basket, wire coil, boat, crucible, and so on. The basket is commonly used to evaporate two different kinds of materials, which are non-adhesive in solid state and adhesive in liquid state. For evaporating non-adhesive materials or expansive materials, the boat is recommended. The crucible is for large quantities or powder types of material. In our study, we used hand made tungsten wire filaments as an evaporation source to evaporate aluminum since the filament shape is easier to make than a basket shape. Figure 4.2 shows commercial wires and hand made tungsten filament. Commercial tungsten baskets or coils did not meet the requirements of the quench condensation because it needed too much electric current to evaporate materials. The disadvantage of high current applied comes from the fact that the wire heated by high electric current boils off the liquid helium too fast.

Figure 4.2 Commercial (left) and hand made (right)

To produce a high quality sample, the amount of applied electrical current becomes an important factor since it determines the evaporation rate. We compared evaporation conditions as adjusting electrical current at room temperature with commercial thermal evaporator. This test allows us to learn how much current is needed for evaporation with the quench-condensation apparatus. Aluminum has been melted for 30 seconds when we applied electrical current of 30A with commercial evaporator. It was completely melted several seconds after the start and the evaporation rate was very large (~20 Hz/sec). Aluminum has started to melt in ~3 minutes with 20A and it completely melted in 30 seconds after start to melt. The evaporation rate was about 6Hz/sec. It takes a long time (7~8 minutes) at 15A. It did not thoroughly melt before the evaporation. The aluminum started to evaporate even if it was not thoroughly melted but just partly melted at its surface. The evaporation rate was about 1~2 Hz/sec. Aluminum did not melt even after more than 20 minutes and did not evaporated for less than 15A. The frequency of the QCM has been increased due to the thermal radiation of the evaporation source heated for a long period. The resonance frequency of the QCM was very unstable and finally it started to fluctuate after 20 minutes. The resonance frequency of the QCM has increased more than 20 Hz and fluctuated between 10Hz of different values. Table 4.1 shows the instability of the resonance frequency of QCM.

Table 4.1 The resonance frequency of QCM for the current of less than 15A

Initial value	After 5 minutes	After 10 minutes	After 15 minutes	16~20 minutes
4.984625 MHz	4.984627 MHz	4.984630 MHz	4.984634 MHz	4.984636~45 MHz (Fluctuating)

Figure 4.3 shows the condition of evaporant after this evaporation test. The evaporation source at the bottom of the Figure 4.3 is the result of not enough current supply.

Figure 4.3 Evaporation source after evaporation

Consequently, the electric current should meet a required amount to get an appropriate evaporation rate. The electric current that is required to heat the evaporant can be obtained by a simple equation.

$$P = I^2 R \tag{6}$$

It is not difficult to get the resistance (R) of the evaporation source if we use some instruments to measure its resistance. But we need to consider several factors to get the power (P) because various thermal effects take place during the evaporation process [15]. The power should be enough to support the heat of melting and the heat of vaporization, the loss of thermal energy by conduction and radiation to the surroundings, the kinetic energy for the evaporated atoms.

The heat required to raise the temperature of the evaporant can be calculated from the simple equation.

$$Q_e = m_e \int_{Ti}^{T_e} C_{p-e} dT \tag{7}$$

whrer m_e is the mass, C_{p-e} is the specific heat of the material to be evaporated and T_e is the temperature at the melting point, T_i is the initial temperature of the material.

The heat for the evaporation source is can be obtained from a similar equation

$$Q_s = m_s \int_{T_i}^{T_e} C_{p-s} dT \tag{8}$$

where m_s is the mass and C_{p-s} is the specific heat of the evaporation source.

The latent heat(Q_l) is also required so the total required heat can be obtained by

$$Q_{tot} = Q_e + Q_s + m_e Q_l \tag{9}$$

We can get the power from these equations with the assumption of that there are no loss of heats by conduction and radiation.

$$I = \sqrt{\frac{P}{R}} = \sqrt{\frac{Q_{tot}}{R\Delta T}} \tag{10}$$

where ΔT is the time to evaporate all materials to be evaporated. But this is not an exact current for the evaporation because we neglected the loss of heats. We can roughly derive the equation for the heat loss by conduction from Fourier's law.

$$\frac{\partial Q_c}{\partial t} = -k \oint_s \Delta T \cdot dS \tag{11}$$

where Q_c is the amount of heat conducted, t is the time taken, k is the conductivity of materials, S is the surface through which the heat is flowing.

We can rewrite this as

$$Q_c = -2kA \frac{dT}{dx} \tag{12}$$

where A is the cross sectional area of the electrodes holding the evaporation source.

The loss of heat by the thermal radiation also needs to be calculated and it can be done by the Stefan Boltzmann's Law

$$W = \sigma \cdot S \cdot T^4 \tag{13}$$

If we assume that the temperature of the evaporation source is uniform then the thermal radiation can be roughly calculated as

$$W = A_s l \sigma (T_s^{\ 4} - T_0) \tag{14}$$

where A_s is the cross sectional area and l is the length, T_s is the temperature of the evaporation source.

The total power required for evaporation can be obtained from equations (9, 12, 13)

$$P_{tot} = \frac{Q_{tot}}{\Delta t} + Q_c + W \tag{15}$$

The electric current that is required is

$$I = \sqrt{\frac{P_{tot}}{R}} \tag{16}$$

4.3 Thickness Measurement

The QCM (quartz crystal microbalance) is one of the famous devices on thin film technology based on the piezoelectric effect. The piezoelectric effect of quartz has been discovered by Jacques Curie and Pierre Curie in 1880. The quartz crystal has some strain when certain electrical voltages are applied. The direction of the strain depends on the electrical voltage direction. Due to this effect, the quartz vibrates when applying an alternating current. This vibration creates a transverse wave, which gives the characteristic resonance frequency of the crystal. The QCM has been used for a long time in many research areas, especially for the measurement of mass change because of its precision and sensitivity of frequency. As one of the applications, a QCM can calibrate the mass which is deposited on the surface of the quartz crystal during the evaporation process in thin film production. It is used not only for thin film technology but also for various research area such as virus detection in biomedical experiments, chemical experiments, and so on. We used the 5MHz QCM to measure the thickness of a sample for this experiment. Figure 4.4 shows a photo and a schematic view of a QCM.

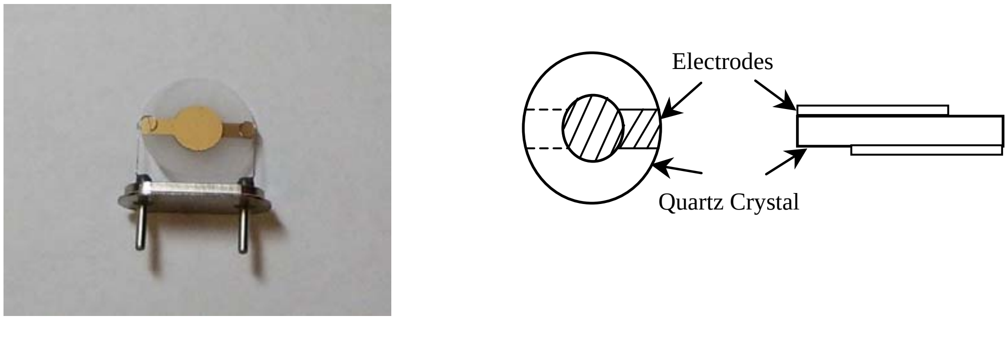

Figure 4.4 Quartz crystal microbalance (QCM)

It was difficult to control the QCM during the quench condensation experiment due to the required conditions of a low temperature experiment. When considering heat flows of the system, it is important to minimize the effect of temperature in order to obtain a stable resonance frequency. At the beginning of this experiment, the frequency of the QCM was fluctuated with the increase of temperature since there was no protection of the QCM from the heat radiation of an evaporation source. The temperature difference between the crystal and electrodes holding the crystal makes the QCM unstable in terms of the resonance frequency [35]. The heat radiation of the evaporation source rapidly increases the temperature of the electrodes that are made of conductors such as gold, silver, and so on. We could have reduced the unstableness of the resonance frequency by making a thermal shield to protect electrodes. Thermal shielded electrodes enhance the stability of the resonance frequency. Figure 4.5 shows photos of the QCM, one is unshielded and another is shielded. We used 4 copper baffles and a stainless box for shielding since more baffles are effective to reduce the thermal radiation.

Figure 4.5 Radiation shield for QCM

After the QCM was immersed into liquid nitrogen, by cooling down the system, the resonance frequency decreases due to the change of elasticity and size of a crystal. The range of resonance frequency covers from 4.987MHz to 4.992MHz as shown in Figure 4.6.

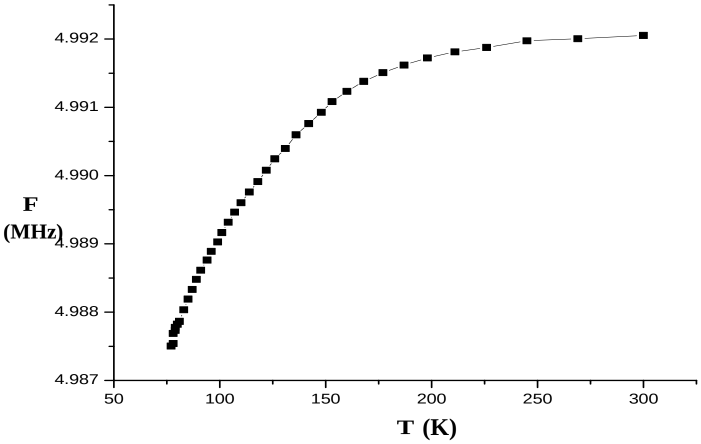

Figure 4.6 Resonance frequency versus temperature of QCM at liquid nitrogen

In general, the QCM shows a stable profile of resonance frequency when it reaches the equilibrium temperature with surroundings. It takes more than one hour to reach the equilibrium state at liquid nitrogen as shown in Figure 4.7.

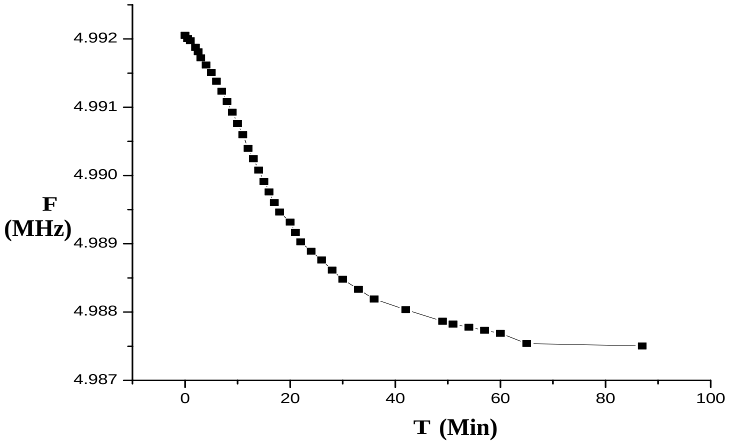

Figure 4.7 Resonance frequency versus time of QCM at liquid nitrogen

As soon as the evaporation source becomes heated up, however, the frequency starts to increase. At liquid nitrogen temperature of 77K, the sensitive behavior of the resonance frequency was unexpectedly observed in terms of changing temperature. A sudden increase of the resonance frequency of QCM was measured. A thermal shield helped to reduce such an increase of the resonance frequency, but it was not enough to remove the thermal effect completely at liquid nitrogen. For a large cryogenic apparatus, a commercial QCM is used since the QCM is stabilized at low temperature by controlling its temperature with heating wire. However, it was difficult to install this QCM in our apparatus since it takes a comparatively large space, which is not good in a compact system. Therefore, we could not use the QCM to measure the evaporation rate. We controlled the evaporation rate by measuring the resistivity of a sample as the material is deposited onto the surface. We have used an in-situ technique that is described in the sample preparation part (Section 4.4) of this thesis. The current required for evaporation was obtained form the equation (12) in the evaporation source part (Section 4.2).

The thickness of the evaporated sample was measured by comparing the resonance frequency of the QCM before and after evaporation. The resonance frequency was transformed to the thickness of sample by means of the Sauerbrey equation.

$$\Delta f = -\frac{2\Delta m f_0{}^2}{A\sqrt{\rho_q \mu_q}} \qquad (17)$$

where f_0 is the resonance frequency of the QCM and A is the active area of the crystal between electrodes that are same as the hole area of the thermal shield in this system. ρ_q is the density of quartz (ρ_q =2.648 g/cm^3) and μ_q is the shear modulus of quartz

(μ_q=2.947310^{11} g/cm3S^2)

The mass of deposited materials can be expected from the equation (17) as

$$\Delta m \approx 4.3 \times 10^5 \frac{A\Delta f}{f_0^{\,2}} \tag{18}$$

Our QCM has a resonance frequency of 5MHz and the active area of the crystal is 0.25cm^2. So the mass change for 1Hz of frequency change is 4.3×10^{-9}g. The thickness of deposited material can be calculated from the following relationship

$$t = \frac{\Delta m}{A\rho_m} = 1.7 \times 10^{-8} \times \frac{1}{\rho_m} \tag{19}$$

where ρ_m is the density of the deposited material. When changing the thickness by (a increase of) 1Å, decrease of the resonance frequency for aluminum (ρ = 2.7 g.cm^{-3}) is 1.58Hz/Å and for nickel (ρ = 8.908 g.cm^{-3}) is 5.26 Hz/Å. It is noted that there is 1.3 cm of gap between the QCM and the substrate of our instrument, which may cause errors in our measurements. The correction can be made by using the density of the deposition flux. Assuming that sample is evaporated isotropically from the evaporation source, there is the relation

$$4\pi R_1^{\,2}\Delta m_1 = 4\pi R_2^{\,2}\Delta m_2 \tag{20}$$

where Δm_1 is the mass change of QCM and Δm_2 is the adjusted mass change.

$$\Delta m_2 = \Delta m_1 \, {R_1^{\,2}}/{R_2^{\,2}} \tag{21}$$

The corrected thickness can be extracted form the equations (19) and (21) as follows

$$t = 1.1 \times 10^{-8} \times \frac{1}{\rho_m} \tag{22}$$

As a result, with increasing thickness of 1Å, decrease of the resonance frequency for aluminum is 2.4Hz/Å and for nickel is 8.0Hz/Å.

4.4 Sample Measurement

We measured the thickness dependent conductivity by means of quench-condensation. We did 4-wire measurements for samples that are evaporated on glass or silicon substrate. The measurements are performed in-situ at ultra-high vacuum condition. Sequential evaporation was performed after measuring the conductivity of a sample at a thickness. The process is repeated until the thin film shows metallic properties.

For measurement of the thickness dependent conductivity, an in-situ experimental technique is much more convenient than ex-situ technique. The reason is that the ex-situ technique requires the fabrication of many samples with different thickness for measuring the thickness-dependency of conductivity. Beside, it is almost impossible to measure the electrical property of ultra thin film by using ex-situ technique because the sample loses its electrical property when ultra thin films are exposed to air. Ex-situ, grains of the thin film start to coalesce and form large islands which are disconnected by heating to room temperature, and then the conductivity reduces to zero. Thin films start to oxidize as well if exposed to the air. Thus, ex-situ treatment causes irreversible changes in the topology of ultra thin films and significantly changes their electrical property. On the other hand, it was convenient for us to measure the thickness-dependent conductivity of ultra thin films with in-situ experiment. For in-situ treatment, the sample does not experience any critical change of electrical property.

We prepared 4 thin gold contacts on a substrate for in-situ measurement by using a commercial thermal evaporator. 3nm of germanium was deposited on silicon or glass substrate and then 20nm of gold was deposited by using shadow mask. Germanium was evaporated because gold does not readily adhere on the silicon or glass substrate. We used two kinds of substrates (silicon and glass) because the thin film has different electrical property depending on the choice of substrate. The uniformity of the thin film, depending on the nature of substrate, results in the modification of electrical property by different choices of substrate. The thin film has different grain sizes, which causes the different electrical properties of the thin film. Wires are connected to gold contacts before evacuating the chamber and then a shadow mask was mounted on the substrate to make a sample in the form of a bar.

Initially a film is evaporated until the conduction is measured. We performed 2-wire measurements with a precision voltmeter until measuring the initial conduction, and then performed a 4-wire measurement. The order of measurement is important to check whether or not the sample initially has infinite resistance that would impose an overload for differential preamplifier. During evaporation, the temperature of the substrate increased by ~10K. Measurement of resistance was performed while cooling down the sample to its initial temperature, and then an evaporation was performed again after the sample had uniform resistance. We repeated the sequential process until the thin film had a certain resistance. Figure 4.8 shows schematics of the process.

Resistivity and conductivity are calculated from the resistance that is measured by the 4-wire measurement. Sheet resistance is also calculated from this. Resistivity is

$$\rho = R\frac{dw}{l} \tag{23}$$

where ρ is resistivity, and R is resistance, d is the thickness of the thin film, and w is the width and l is the length of thin film. Conductivity is $\sigma = 1/\rho$ and sheet resistant is $R_s = \rho/d$.

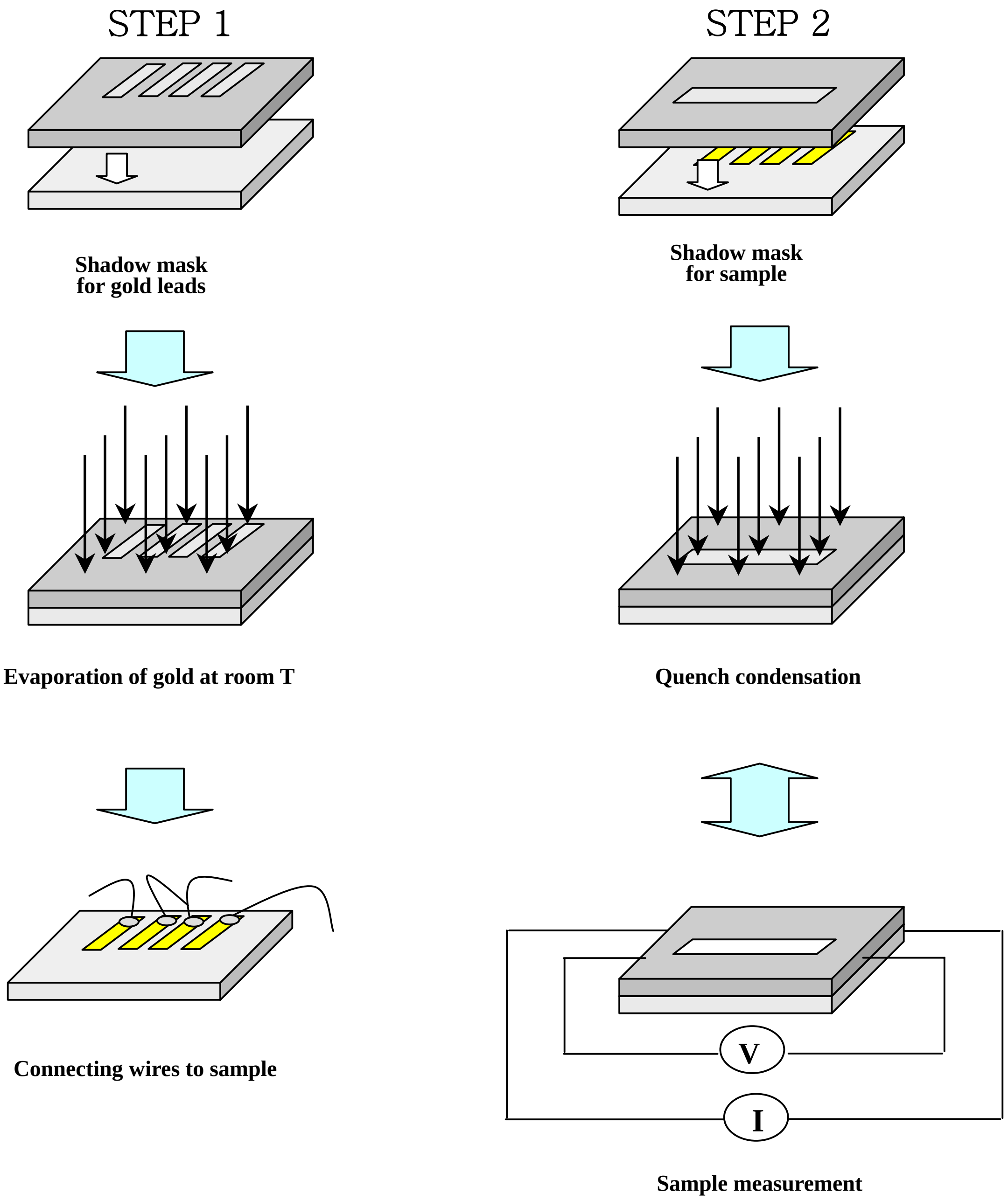

Figure 4.8 Sample preparation and measurement process

CHAPTER V

EXPERIMENTAL RESULTS AND DISCUSSION

5.1 Experimental Results

5.1.1 Evaporation of Aluminum at Liquid Nitrogen

Aluminum thin films were deposited onto a silicon substrate and a glass substrate at 77°K. Sequential evaporations and in-situ measurements were performed with the quench condensation apparatus. The temperature of the substrate was maintained at 77K before and after the evaporation but it rose to ~86K during the evaporation. A vacuum was always maintained during the experiment.

Initially, we evaporated aluminum onto a silicon substrate until we measured a finite conductivity of the thin film. The resistance of the thin film was 1385kΩ at 82.4K but it rapidly increased with time until 1437 kΩ and then its conduction disappeared (Figure 5.1).

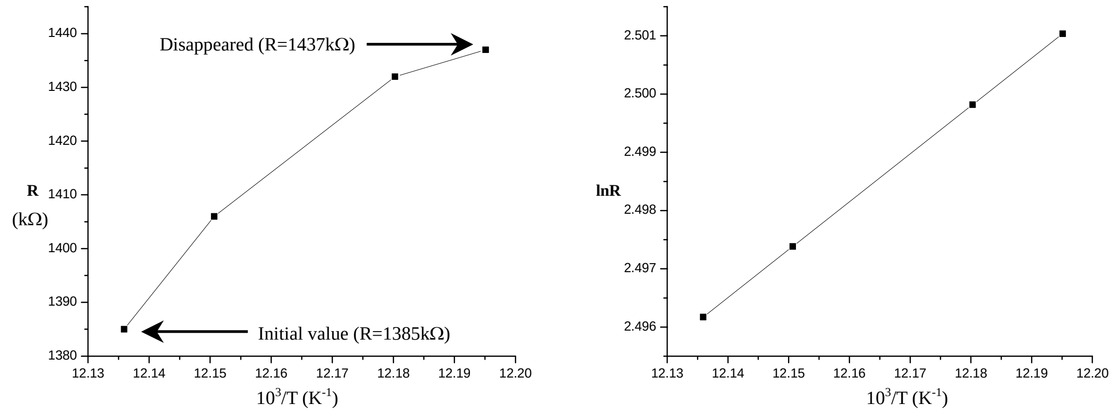

Figure 5.1 Resistance versus temperature for 1st evaporation

After the second evaporation, we did 7 sequential evaporations and in-situ measurements. Figure 5.2 presents these data for films of various thicknesses for the temperature range 77<T<86K. The notations in the figure show the varying thicknesses which increase from *d1* to *d7* (*d1* is the thickness for the 2nd evaporation while *d7* is for the 8th). This figure shows conductivity (σ/σ_0) dependent upon inverse temperature in analogy with the result of Kazmerski and Racine for Au thin films [14]. The temperature dependent variation of conductivity (σ/σ_0) decreased for thicker films.

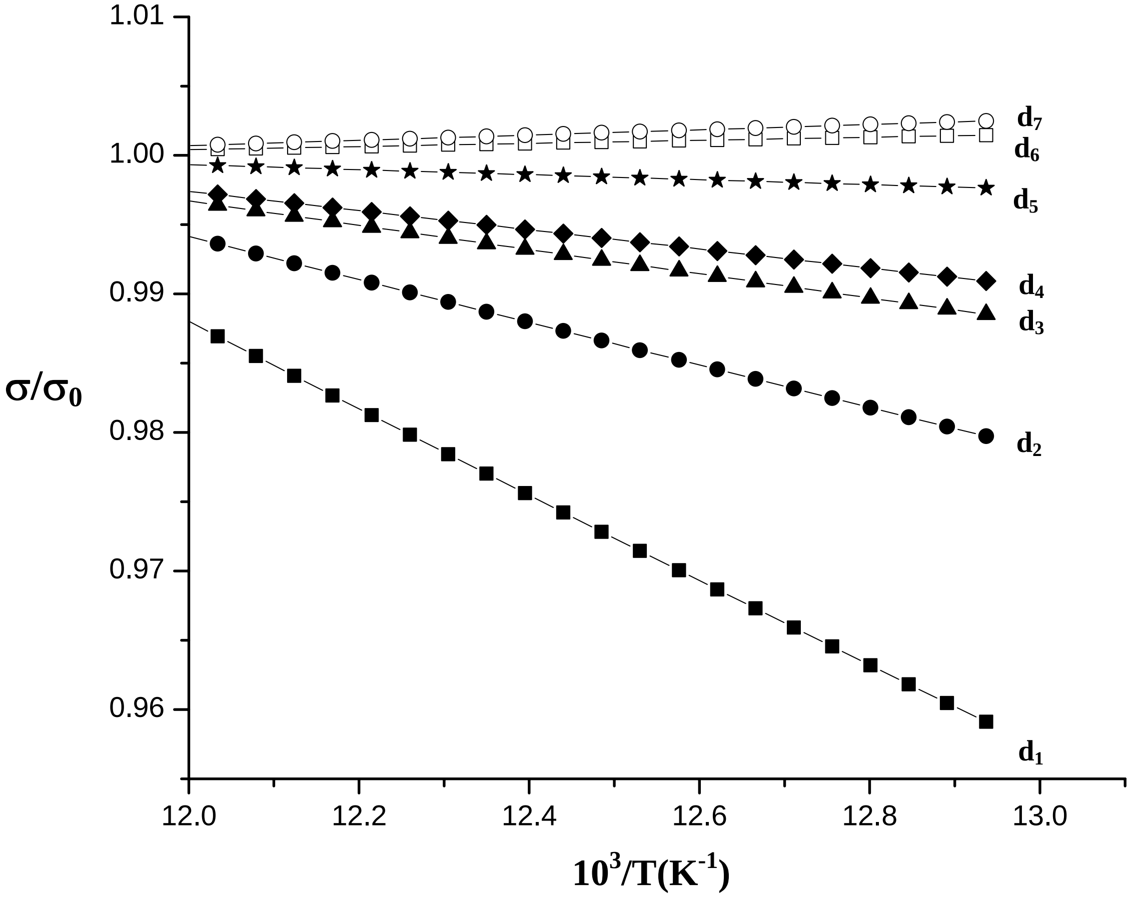

Figure 5.2 The increasing rate of conductivity to depend on inverse temperature

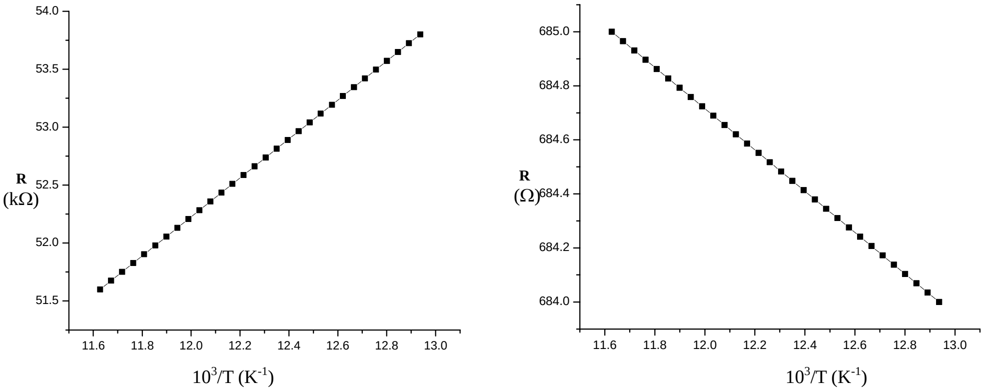

Figure 5.3 Resistance versus inverse temperature for d_1 (left) and d_6 (right)

Figure 5.3 shows the temperature dependence of resistances for thickness d_1 (thickness for the 2nd evaporation) and d_6 (thickness for the 7th evaporation). The resistance increased when cooling the sample for the thicknesses of d_1~d_5 while it decreased for the thicknesses of d_6~d_7. Figure 5.4 shows the natural logarithm of resistance (ln*R*) for thickness d_1 and d_6. This figure shows ln*R* to depend linearly on inverse temperature ($1/T$) that is the result predicted by the Neugebauer and Webb conduction model [5]. In order to conclusively decide on the ln*R* dependence a wider range of T should be measured.

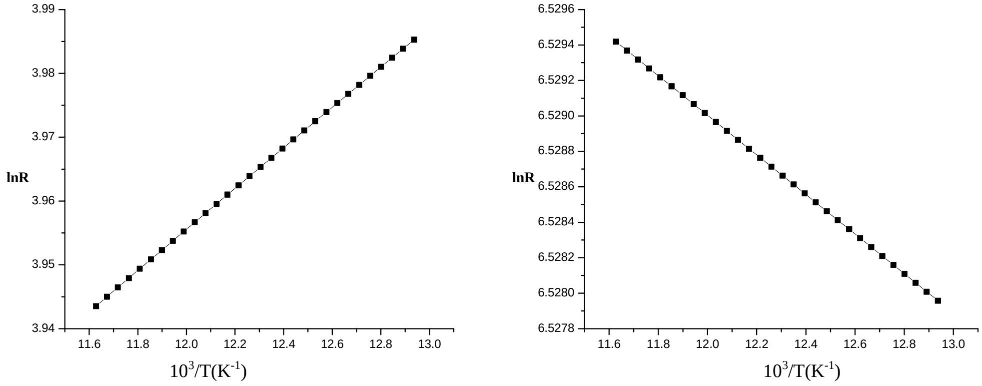

Figure 5.4 Logarithmic resistance (*lnR*) versus inverse temperature for d_1 and d_6

Other results for thickness of d_2~d_6 are exhibited in Figure 5.5 and Figure 5.6. The resistance and ln*R* to depend on inverse temperature are showed for each thickness.

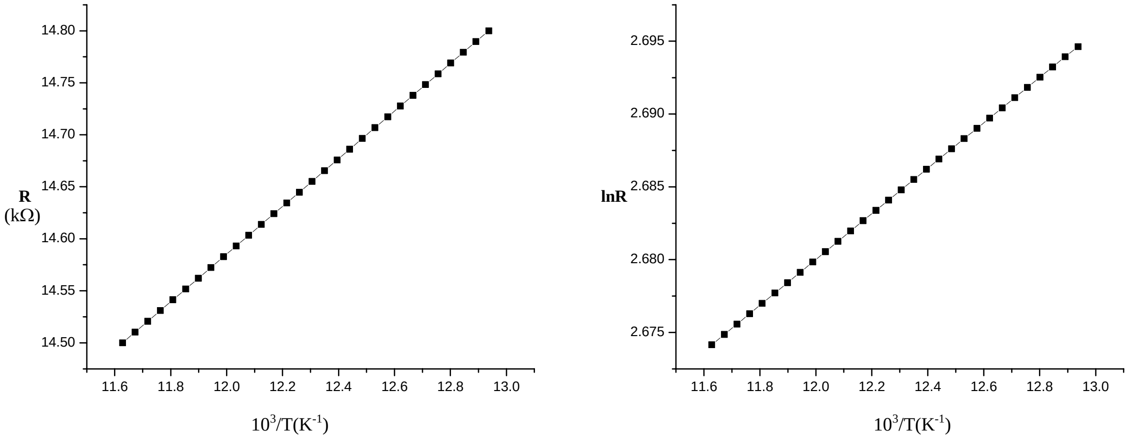

(a) d_2 (b) d_2

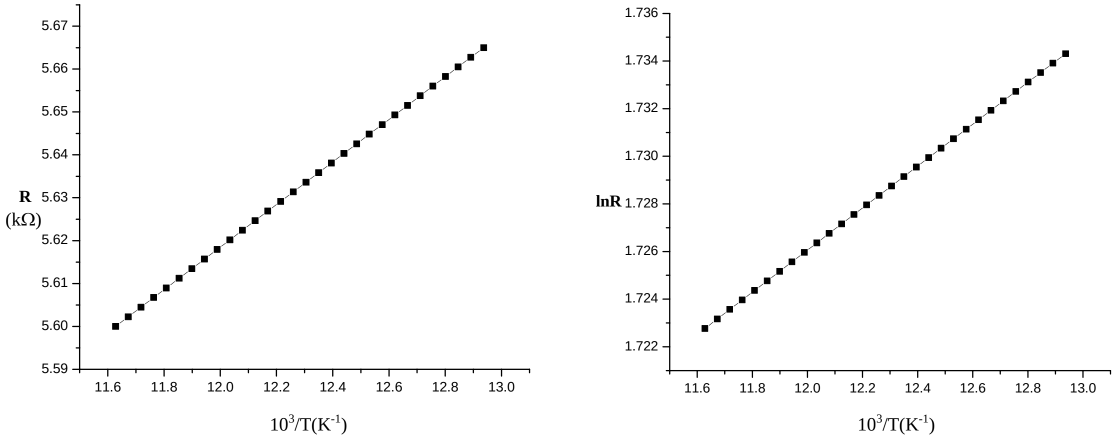

(c) d_3 (d) d_3

Figure 5.5 Resistance and ln*R* versus inverse temperature for d_2 (a) ~ d_3 (d)

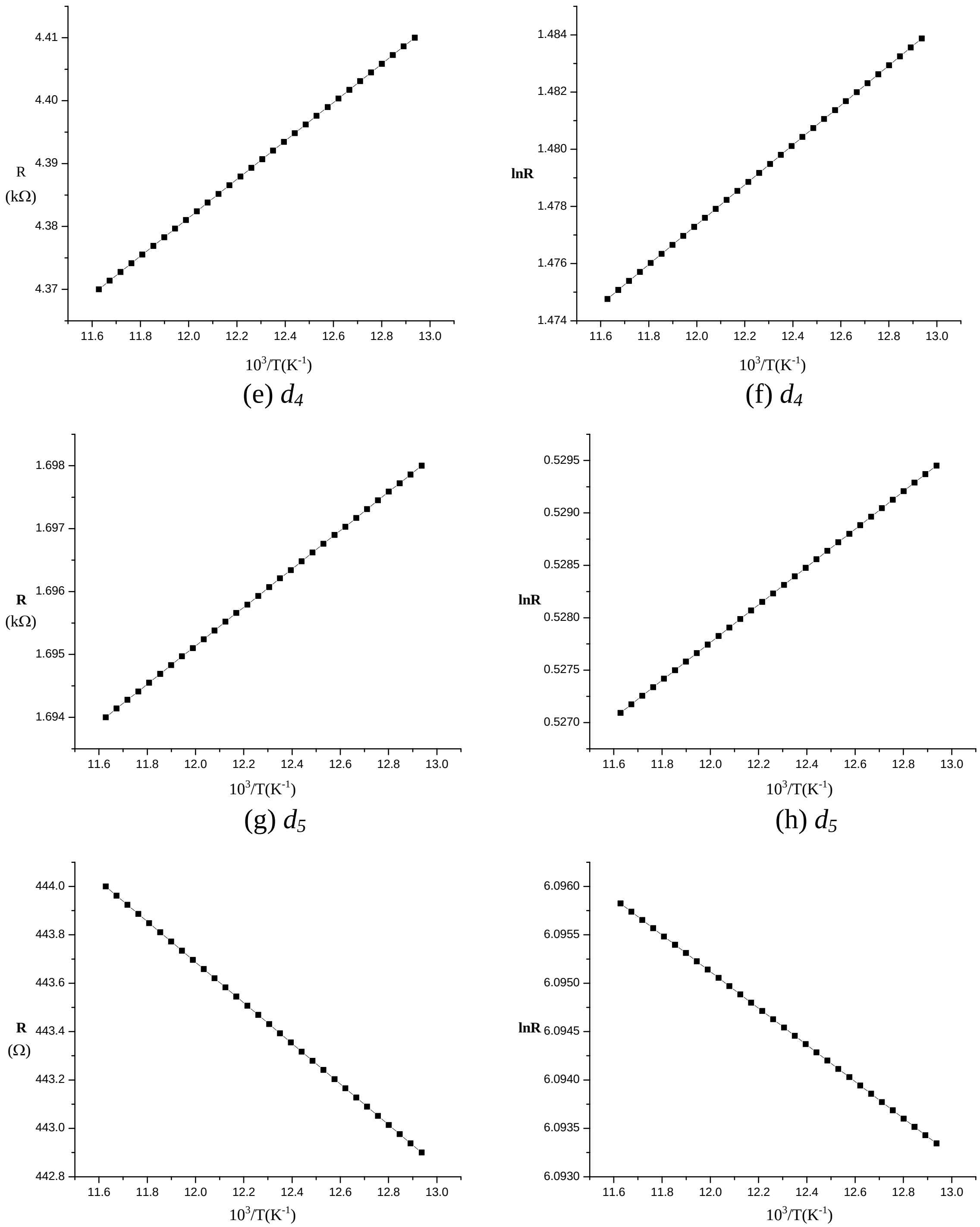

(e) d_4

(f) d_4

(g) d_5

(h) d_5

(i) d_6

(j) d_6

Figure 5.6 Resistance and ln*R* versus inverse temperature for d_4 (e) ~ d_6 (j)

For a thin film on a glass substrate, the initial resistance we measured was much bigger than the deposition on a silicon substrate. As Figure 5.7 shows, we measured 73MΩ as an initial resistance with an underlying glass substrate which is much bigger than 1385kΩ in case of an underlying silicon substrate at Figure 5.1. The resistance initially had increased depended on temperature but it continued to increase after the sample was cooled to 77K. As Figure 5.7 shows, the resistance was increasing for more than 1 hour.

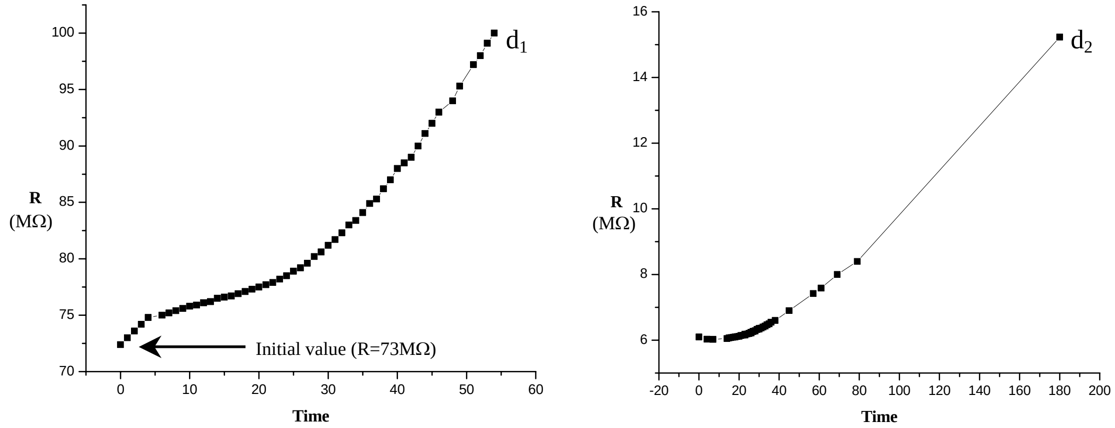

Figure 5.7 Resistance versus time for d_1 (left) and d_2 (right), is deposited on a glass

Figure 5.8 shows an abrupt increase of the resistance after following the linear dependence of logarithmic scale of the resistance (ln*R*) on *1/T* between the dotted lines of Figure 5.9. The temperature dependent increase of resistance becomes smaller as the film thickness was increased.

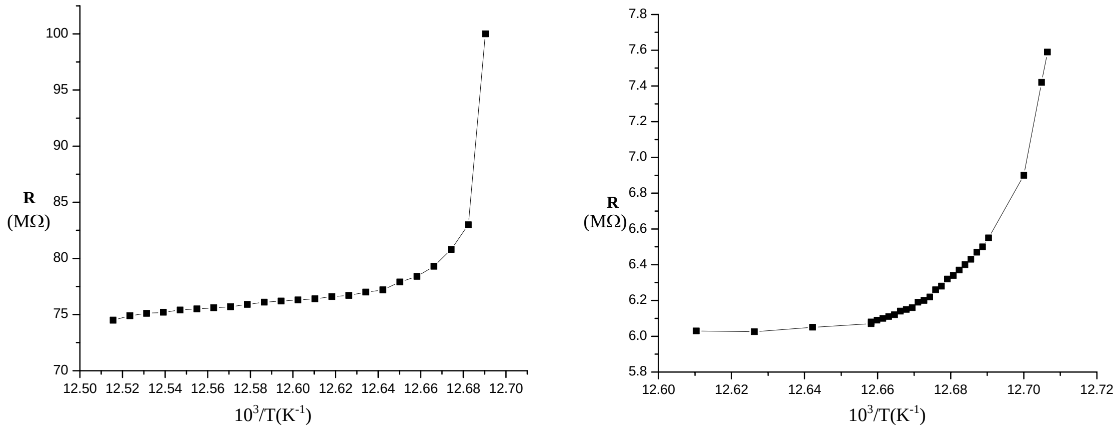

Figure 5.8 Resistance versus temperature for d_1 (left) and d_2 (right)

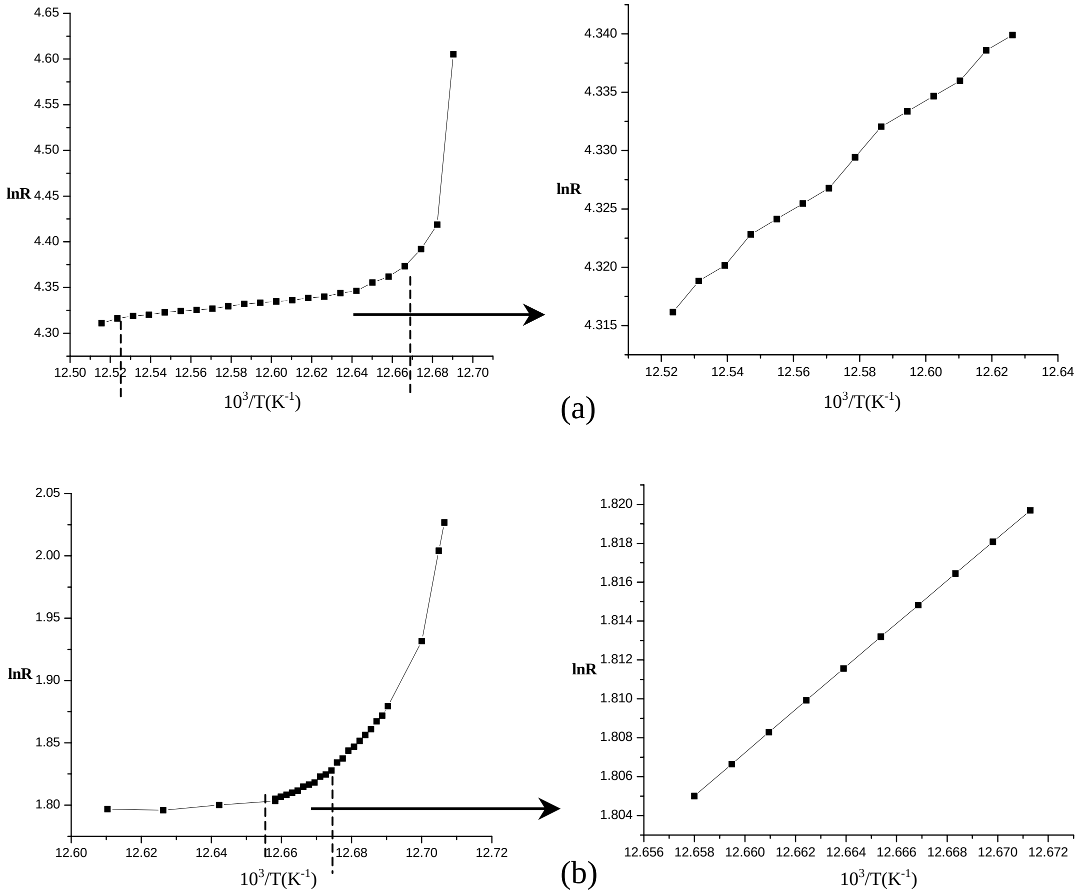

(a)

(b)

Figure 5.9 ln$R$ versus temperature for d_1 (a) and d_2 (b). The plot at right side is a linear dependent part of the plot at left side (between dotted lines).

5.2 Discussion

5.2.1 Linear dependence of ln*R* and lnσ on *1/T*

As we introduced in Chapter II (Background), the model of Neugebauer and Webb [5] agree very well with experimental results. In this model, the conductivity of thin film was explained by tunneling between islands. The conductivity is given by the equation (3) in chapter 2.

$$\sigma \propto \frac{1}{r} d^2 q^2 D \exp\left(-\frac{q^2 / r}{kT} \right) \tag{3}$$

From this, we can predict the linear dependence of the logarithmic conductivity on inverse temperature as

$$\ln \sigma \propto -\frac{1}{T} \tag{24}$$

The resistance has relations as

$$R \propto \rho \propto \frac{1}{\sigma} \tag{25}$$

and

$$R \propto \frac{r}{d^2 e^2 D} \exp\left(\frac{e^2 / r}{kT} \right) \tag{26}$$

Due to this equation, the logarithmic conductivity depends on inverse temperature

$$\ln R \propto \frac{1}{T} \tag{27}$$

The experimental data shows the linear dependence of ln*R* on inverse temperature except for some abrupt increase for the deposition on a glass substrate. The slope of the linear dependence of conductivity (σ/σ_0) on temperature was varying with thickness as shown at

Figure 5.2. This can be expected from the equation (26) by modify some parameters as

$$\sigma = C(d/r)\exp\left(A/\varepsilon rkT - Bd\right) \tag{28}$$

where A is a function of e^2 and ε is an effective dielectric constant of the media between islands. C and B are constant which depend on the potential (V) of the tunneling barrier (C, $B \propto qV$). Due to equation (28), the slope of the plots in Figure 5.2 is decreasing with the thickness of the sample since the exponential terms of the equation becomes constant by increase of the effective island size r during the growth of the sample. As Figure 5.3 and 5.4 show, the resistance also depends almost linearly on inverse temperature. This is due to the fact that the temperature range ($77 < T < 86$K) was too narrow to show the obvious logarithmic curvature. The preciseness of the temperature calibration can also affect the curvature.

5.2.2 Initial Value of the Resistance

As Figure 5.1 and 5.7 show, the initial resistance of the deposition on a glass substrate was different from the deposition on a silicon substrate. This can be explained in several ways depending on substrates as the saturation ratio, the surface roughness, and electrical effect of silicon substrate.

(a) Surface roughness

The surface roughness of a substrate results in different growth conditions of a thin film. Since the surface of a silicon substrate is comparatively smooth and uniform the aluminum forms a uniform thin film on the silicon substrate. On the other hand, the glass substrate has a comparatively rough surface unless it has been polished to be smooth. Thus the aluminum forms a rough thin film on the glass substrate. This should increase the inter island separation (*d*) and finally increase the resistance of thin film.

(b) Electrical effect of silicon substrate

The silicon has some conductivity (being a semiconductor) while the glass has very poor conductivity, being an insulator. It is possible that the SiO_2 layer of the silicon substrate was saturated with aluminum during the deposition and formed some mixed layer on the boundary between the thin film and the substrate. This effect is a task of future work and will not be discussed in detail. If the aluminum is mixed with the SiO_2 layer on the boundary by saturation then it can affect the conductivity of thin film. The tunneling area can be changed by variation of the dielectric constant between the grains of the thin film. More over, the conductivity can be increased by the addition of surface impurities after the aluminum is mixing with the silicon at the boundary of substrate [36].

5.2.3 Abrupt Increase of the Resistance

As Figure 5.8 shows, an abrupt increase of the resistance during the deposition of aluminum on the glass substrate. This can be explained by the contamination of the ultra-thin film and substrate through the adsorption of oxygen at the film surface [14, 36]. Fehlner has described the increase of resistance of zirconium films [37] by oxidation. At a pressure of 10^{-7} torr, which is lower than the pressure of our experiment when evaporating aluminum at liquid nitrogen, the oxygen formed a monolayer on the island of the thin film and then it increased the resistance sharply. Kazmerski and Racine had a similar experimental result and explained this with the varying of the effective tunneling distance, which is the same as the inter island separation (*d*), due to the adsorption of oxygen [14]. As Figure 5.10 shows, oxygen forms a thin monolayer of Al_2O_3 on the island which increases the resistance of the thin film by increasing the tunneling barrier between islands.

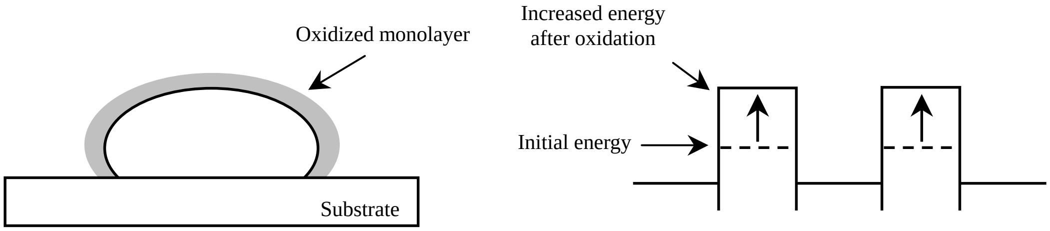

Figure 5.10 Increase of the tunneling barrier by oxidation of thin film

Lazarov and St. Manev have found oxygen absorption by a discontinuous gallium thin film at 77K.

It is likely that the abrupt increase of resistance of our experimental data is due to the oxidation of the aluminum thin film. During the deposition of aluminum on the glass substrate, the vacuum level of the chamber was less than 10^{-6} and the thin film was left for a long time (t > 1hour) after evaporation. This was a comparatively long time and aluminum is comparatively easy to oxidize. Some outgassing may also be produced during the measurement and then the thin film was oxidized.

It is important to notice that the evaporation at liquid nitrogen is not appropriate for sequential in-situ experiments on aluminum unless the turn-around time of evaporations and measurements is very quick. This may similar for the evaporation of nickel. Even if we can get a better quality of thin film from the evaporation at liquid nitrogen than from the evaporation at room temperature, the quality is limited to a certain level. On the other hand, the oxidation of a thin film is significantly reduces when quench-condensing at liquid helium since the system maintains an ultra-high vacuum by cryopumping of the apparatus.

CHAPTER VI

CONCLUSION

The growth process and the electrical properties of a thin film were investigated by using the newly designed apparatus at liquid nitrogen. Especially the dependence of non-metallic behaviors was investigated by means of the in-situ measurement. The apparatus has potential to be used for many experiments in the future. Due to its ability to perform in-situ experiment at low temperature, it was convenient for experimental results on ultra-thin films.

The temperature was too high to quickly quench-condense the evaporated materials on the substrate to form a uniform thin film. The vacuum pressure produced by cryopumping of liquid nitrogen and room temperature pumping with the diffusion pump was not enough to completely protect the sample from the oxidation during the sequential evaporations.

Some additional experiments will need to be performed until this experimental technique is optimized. In the future work, we will investigate the electrical properties of thin films at liquid helium by applying the quench-condensation technique to fabricate nickel thin film. Once successful, we will continue to investigate the magnetic field driven metal-insulator transition.

REFERENCES

[1] W. Teizer, F. Hellman, and R. C. Dynes, Phys. Rev. Lett. **85**, 848 (2000).

[2] W. Teizer, F. Hellman, and R. C. Dynes, Solid State Commun. **114**, 81 (2000).

[3]. A. Frydman, Physica C **391**, 189(2003)

[4]. A. Frydman, O. Naaman, and R. C. Dynes, Phys. Rev. B. **66**, 052509 (2002)

[5]. C. A. Neugebauer and M. B. Webb, J. Appl Phys. **33**, 74 (1962)

[6] A. A. Milgram and C. S. Lu, J. Appl Phys. **37**(13) 4773 (1966)

[7] P. Sheng, B. Abeles and Y. Arie, Phys. Rev. Lett. **31**, 44 (1973)

[8] B. L. Altshulter and A. G. Aronov, P. A. Lee, Phys. Rev. Lett. **44**, 1288 (1980)

[9] J. K. Graybeal and M. R. Beasley, Phys. Rev. B. **29**, 4167 (1984)

[10] H. M. Jaeger, D. B. Haviland, B. G. Orr, and A. M. Goldman, Phys. Rev. B. **40**, 182 (1989)

[11] Matthew P. A. Fisher, Phys. Rev. Lett. **65**, 923 (1990)

[12] M. Strongin, R. S. Thompshon, O. F. Kammerer and J. E. Crow, Phys. Rev. B. **1**, 1078 (1970)

[13] G. J. Dolan and D. D. Osheroff, Phys. Rev. Lett. **43**, 721 (1979)

[14] L. L. Kazmerski and D. M. Racine, J. Appl Phys. **46**, 791 (1975)

[15] K. S. Sree Harsha, *Principles of Physical Vapor Deposition of Thin Films* (Elsevier, Boston, 2006)

[16] A. E. Riad and F. D. Barlow III, *Thin Film Technology Handbook* (McGraw-Hill, New York, 1997)

[17] D. G. Naugle, B. Bandyopdhyay, Yin Bo, V. M. Nicoli, R. C. Wang, and D. Rathnayaka, Rev. Sci. Instrum. **58**, 1271 (1987)

[18] L. M. Hernandez and A. M. Goldman, Rev. Rev. Sci. Instrum. **73**, 162 (2002)

[19] M. Curry, D. Arrington and S. C. Street, J. Vac. Sci. Technol. A **21**(1), 234 (2003)

[20] M. Zinke-Allmang, L. C. Feldamn, S. Nakahara, and B. A. Davidson, Phys. Rev. B. **38**, 7848 (1989)

[21] A. Raab and G. Springholz, Appl. Phys. Lett. **77**, 2991 (2000)

[22] R. C. Dynes, J. P. Garno, and J. M. Rowell, Phys. Rev. Lett. **40**, 479 (1978)

[23] B. G. Chae, H. T. Kim, S. J. Yun, B. J. Kim, Y. W. Lee, and K. Y. Kang, J. J. App. Phys. **46**, 738 (2007)

[24] N. F. Mott, Rev. Mod. Phys.**40**, 677 (1968)

[25] F. Gebhard, *The Mott Metal-Insulator Transition* (Springer Berlin, Heidelberg, 2000)

[26] D. J. Scalapino, S. R. White and S. Zhang, Phys. Rev. B. **47**, 7995 (1993)

[27] M. Oshikawa, Phys. Rev. Lett. **90**, 236401 (2003)

[28] T. Ihn, *Electronic Quantum Transport in Mesoscopic Semiconductor* (Springer Berlin, Heidelberg, 2004)

[29] E. I. Zornberg, Phys. Rev. B. **1**, 244 (1970)

[30] G. S. Painter, D. E. Ellis and A. R. Lubinsky, Phys. Rev. B. **4**, 3610 (1971)

[31] N. F. Mott, *Metal-Insulator Transition* (Taylor & Francis Ltd, New York, 1974)

[32] E. D. Black and John C. Price, Phys. Rev. B **58**, 7844 (1998)

[33] R. C. Richardson and E. N. Smith, *Experimental Techniques in Condensed Matter Physics at Low Temperatures* (Addision-Wesley, Redwood City, CA, 1988)

[34] G. K. White and P. J. Meeson, *Experimental Techniques in Low-Temperature Physics* (Oxford University Press, Oxford, 2002)

[35] L. Bouzidi, S. S. Narine, K. G. Stefanov, and A. J. Slavin, Rev. Sci. Instrum. **74**, 3039 (2003)

[36] J. E. Morris and T. J. Coutts, Thin Solid Films. **47**, 3 (1977)

[37] F. P. Fehlner, Nature. **210**, 1035 (1966)

VITA

Kyoungjin Lee was born in 1978 in SeongNam, The Republic of Korea. He received a B.S. in applied physics from the Korea Military Academy in 2001, then he was commissioned as a Artillery officer. He served in the ROK Army from 2001 to 2004 as a fire battery leader and staff officer. He entered the Physics Department at Texas A&M University in 2005 as an M.S. student and graduated in August 2007.

Permanent Address: 73-1 Hyeonbang-Ri Baeksa-Myon
Ichen, Gyonggi-Do, 467-830, Republic of Korea.

E-mail Address: lee6457@neo.tamu.edu